

This is an Open Access document downloaded from ORCA, Cardiff University's institutional repository:<https://orca.cardiff.ac.uk/id/eprint/131769/>

This is the author's version of a work that was submitted to / accepted for publication.

Citation for final published version:

Li, Benxuan, Lu, Mingxia, Feng, Jiangtao, Zhang, Jingchao, Smowton, Peter M , Sohn, Jung Inn, Park, Il-Kyu, Zhong, Haizheng and Hou, Bo 2020. Colloidal quantum dot hybrids: an emerging class of materials for ambient lighting. *Journal of Materials Chemistry C* 8 (31) , pp. 10676-10695. 10.1039/d0tc01349h

Publishers page: <http://dx.doi.org/10.1039/d0tc01349h>

Please note:

Changes made as a result of publishing processes such as copy-editing, formatting and page numbers may not be reflected in this version. For the definitive version of this publication, please refer to the published source. You are advised to consult the publisher's version if you wish to cite this paper.

This version is being made available in accordance with publisher policies. See <http://orca.cf.ac.uk/policies.html> for usage policies. Copyright and moral rights for publications made available in ORCA are retained by the copyright holders.



# Colloidal Quantum Dot Hybrids: An Emerging Class of Materials for Ambient Lighting

Benxuan Li<sup>a,§</sup>, Mingxia Lu<sup>b,§</sup>, Jiangtao Feng<sup>c,§</sup>, Jingchao Zhang<sup>d</sup>, Peter M Smowton<sup>e</sup>, Jung Inn Sohn<sup>f,\*</sup>, Il-Kyu Park<sup>g,\*</sup>, Haizheng Zhong<sup>h,\*</sup> and Bo Hou<sup>e,\*</sup>

<sup>a</sup>Electrical Engineering Division, Engineering Department, University of Cambridge, 9 JJ Thomson Avenue, Cambridge CB3 0FA, United Kingdom

<sup>b</sup>School of Chemistry and Chemical Engineering, Henan University of Technology, Zhengzhou 450001, P. R. China

<sup>c</sup>Department of Environmental Science & Engineering, State Key Laboratory of Multiphase Flow in Power Engineering, Xi'an Jiaotong University, Xi'an, 710049, P.R. China

<sup>d</sup>Department of Biostatistics and Bioinformatics, Emory University, Atlanta, GA, 30322, USA

<sup>e</sup>Department of Physics and Astronomy, Cardiff University, Cardiff CF24 3AA, United Kingdom

E-mail: [HouB6@cardiff.ac.uk](mailto:HouB6@cardiff.ac.uk) (B.H.)

<sup>f</sup>Division of Physics and Semiconductor Science, Dongguk University-Seoul, Seoul, 04620, Republic of Korea

E-mail: [junginn.sohn@dongguk.edu](mailto:junginn.sohn@dongguk.edu) (J.I.S.)

<sup>g</sup>Department of Materials Science and Engineering, Seoul National University of Science and Technology, Seoul 139-743, Republic of Korea

E-mail: [pik@seoultech.ac.kr](mailto:pik@seoultech.ac.kr) (I.K.P.)

<sup>h</sup>Beijing Key Laboratory of Nanophotonics and Ultrafine Optoelectronic Systems, School of Materials Science & Engineering, Beijing Institute of Technology, 5 Zhongguancun South Street, Haidian District, Beijing 100081, China

E-mail: [hzzhong@bit.edu.cn](mailto:hzzhong@bit.edu.cn) (H.Z.)

## Abstract

The rapid growth of the global economy and urbanization have resulted in major worldwide issues such as greenhouse gas emission, air pollution and energy crisis. Artificial ambient light is one of the great inventions in human's history, but it is also one of the primary energy consumption constituents and a focus of the global energy grand challenge. Therefore, low cost and low energy consumption lighting technology is in high demand. In this review, we will summarise and prospect one of the emerging lighting technologies-white electroluminescence light-emitting diodes enabled from hybrid colloidal quantum dots (WQLEDs), which have attracted intense attention since promising potential in both flat-panel backlighting and solid-state lighting. WQLEDs have unique high luminescence efficiency, broad colour tunability and solution processability. Over the past decades, the development of colloidal quantum dot synthesis, material engineering and device architecture highlight the tremendous improvement in WQLEDs formation. As WQLEDs efficiencies approach those of

molecular organic LED, we identify the critical scientific and technological challenges and provide an outlook for on-going strategies to overcome these challenges.

## 1. Introduction

Energy consumption and the emission of greenhouse gasses have been grand global challenges ever since the Kyoto protocol in 1997. Technological advances in saving energy have drawn considerable attention from the general public, government, industry and academia. Lighting accounts for 22% of electricity use and 8% of all energy use in the United States. In the UK about 8 TWh energy was consumed by different types of lighting in 2018. Conventional lighting methods result in massive energy waste due to their inferior power conversion efficiency, which indicates the replacement with novel lighting technology such as energy-efficient light-emitting diodes (LEDs) can directly contribute to the reduction of energy consumption as well as building environmental-friendly societies. For instance, solid-state lighting (SSL), such as semiconductor LEDs, had already led to reduced electricity usage in the United States and could reduce the electricity used for lighting by 33% in the next decade.

The use of colloidal quantum dots (QDs), as emissive materials, is gaining massive attention in SSL, especially as potential materials employed in white light-emitting diodes (WLEDs) which have potential to replace current high energy-consumption lighting sources such as incandescent and fluorescence lamps.<sup>1, 2</sup> QDs are promising semiconductor nanocrystals with several unique physical and chemical properties, such as outstanding band-gap tunability, high photoluminescence quantum yield (PLQY), narrow linewidth and well solution processability.<sup>3-7</sup> These properties of QDs have motivated increasingly intensive research aimed at applying them in the next generation of optoelectronics, including light-emitting diodes (LEDs)<sup>8-10</sup>, solar cells<sup>11-16</sup>, photodetectors<sup>15, 17</sup>, and field-effect transistors<sup>11, 18, 19</sup>. In fact, with high colour purity and wide colour gamut, televisions, monitors and tablets containing QDs have already appeared and are beginning to thrive in the consumer market.<sup>20</sup> Remarkably, over the past decades, the performance of QD-based light-emitting diodes (QLEDs) has been substantially improved through innovative attempts such as novel designs of QD materials<sup>21-23</sup>, development of charge transport layers and innovation of device architecture<sup>9, 24-26</sup>. For instance, Cd-based high-performed blue, green monochromic QLEDs have been fabricated, while red devices presented the record-high EQE of 20% according to a theoretical limit.<sup>8, 22, 26</sup> In parallel, investigation on the multicoloured QLEDs has been implemented for their general application to ambient lighting.<sup>27-31</sup> With that development, the future of QD based WLEDs (WQLEDs) can be visualized. In this short review, we are going to present the progress and perspective of using QDs for WQLEDs applications.

There are two main approaches to generating white emission through WQLEDs. The first, and currently mainstream, approach relies on a combination of converted blue light from chip and remaining transmitted blue light to generate white emission. This strategy is known as phosphor-converted WQLEDs (pc-WQLEDs). At an early stage,

the photoluminescence (PL) emission of colloidal QDs was mainly used in SSL sources in the display backlighting. Many comprehensive reviews on this topic have been published, from conversion materials to devices, particularly the latest applications of perovskite QD materials.<sup>32-38</sup> The second approach, which may prove superior in the longer term, is the development of white electroluminescence (EL) emission from colloidal QD LEDs, which is being pursued academically and commercially.<sup>6, 9, 39</sup>

This review mainly focuses on the EL mode approach to WQLEDs, with mention of pc-WQLEDs. We firstly give a brief tutorial to the fundamental colour science of WQLEDs, including the principles of human white light perception, the figures of merit for metrics, spectrum and characteristics of current white-lighting technologies and working mechanism of PL mode WQLEDs and EL mode WQLEDs. We discuss cases for, and challenges in, the use of QD materials for fabrication of PL mode WQLEDs. We summarize device architectures in Cd-bases EL WQLEDs from initial single hybrid-QDs to more complex tandem structure as well as heavy-metal-free QD-based WQLEDs such InP, Cu-chalcogenide-based and perovskite-based WQLEDs. In the end, we prospect some potential solution to better performance WQLEDs seeking to connect current academic achievement to the practical realization of WQLEDs for highly efficient ambient lighting.

## **2. Foundation of WQLEDs**

### **2.1 What is ambient white light**

Ambient white light can be defined as a mixture of different wavelength of photons primarily in the visible spectrum. As Newton described, if we have all the rainbow colour light and focus into one spot, then a white light can be obtained. Or by refracting a white light, a beam of white light can be converted to a rainbow-colour spectrum. Generally, white light can be generated from a variety of sources, such as the Sun and many other artificial sources.<sup>40, 41</sup> White light may be used for lighting in our daily life, but it can also be applied in another scenario such as optical communication.<sup>42-44</sup>

### **2.2 The metrology lighting source**

Before we go for comparison of different lighting technology, it is necessary to go through several key parameters that are used to characterise WQLEDs. The efficiency of white lighting source is quantified by the ability to generate a visual sensation, called luminous efficacy (LE). LE is based on convolution of spectral power distribution (SPD) with the spectral sensitivity of the human eye, which peaks in the green range at 550 nm. LE is calculated by taking the generated visual sensation to the power used to produce light, and it is expressed in lumens per watt, instead of in percentage. As seen in eq. 1, the photometric equivalent to the radiant flux is the luminous flux  $\Phi_V$  and according to the definition, LE is expressed in eq. 2.

$$\Phi_V = \frac{683 \text{lm}}{\text{W} \int_{380}^{780} V(\lambda) S(\lambda) d\lambda} \quad (\text{eq. 1})$$

$$\eta_V = \frac{\Phi_V}{P} \quad (\text{eq. 2})$$

Where  $V(\lambda)$ ,  $S(\lambda)$  and  $P$  denote to human eye sensitivity, spectral power distribution and consumed power, respectively.

The sensation of white lighting colour is complicated to determine, but it can be defined by chromaticity coordinates, colour temperature and colour rendering. As shown in Fig. 1a, chromaticity coordinates usually quantify the radiation of colour, and their values can be calculated using tristimulus values X, Y, Z obtained by integrating the spectrum with the standard colour-matching functions x, y, z from a standard observer. (introduced by Commission Internationale de l'Eclairage (CIE) in 1931), as shown in eq. 3. Thus, for the constant energy white point on the CIE chromaticity diagram, it was expected that  $x = y = z = 1/3$ .

$$x = \frac{X}{X + Y + Z}, y = \frac{Y}{X + Y + Z}, z = \frac{Z}{X + Y + Z} = 1 - x - y$$

The correlated colour temperature (CCT) of a light source is the temperature of an ideal black body radiator, determined by Planck's law that radiates light of comparable hue to that light source. White light may be classified as being warm, neutral and cold concerning the emission of ideal white light reference. As the temperature of typical black body increases from 2000 K to 10000 K, the emitted white light shifts from lower colour temperatures (2700–3000 K), called "warm-white" (yellowish), to neutral-white (3500-4000 K) and to the temperatures over 5000 K which are called "cool-white" (bluish).

Colour-rendering index (CRI) is another crucial parameter representing the ability to regenerate object colours as viewed under an ideal white light source, such as standardized daylight and Planckian radiator. By illuminating eight test colour samples and six supplementary ones selected from the colour palette introduced by MUNSSELL, first with an ideal white-light source, then with the white-light source of interest, it is possible to quantify the deviation in reflected spectra.<sup>45, 46</sup> According to this definition, sunlight and incandescent bulbs have a CRI value of 100, which is ideal, and values above 80 are typically regarded sufficient for indoor white lighting. In general, the higher the CRI value, the lower the possible LE because of the human visual repose peaks at 550 nm. This means 550 nm light would have a very high LE of radiation (683 lm/W according to eq. 1) but would just render the objects that can reflect at 550 nm wavelength. Hence, we can also presume there is a trade-off: the wider the spectrum, the better colour rendering value but lower the luminous efficacy.

### 2.3 Spectrum and characteristics of different artificial white light

Since the development of incandescent light bulbs in the late 1800s, various methods

have been investigated for producing white light as an ambient lighting source. The incandescent bulbs are cheap, with a well-established manufacturing process. Even though their LE has improved from 1.51 lm/W to 16 lm/W, the majority of their energy is transformed into heat, limiting the device efficiency. The fluorescent light bulb is another conventional and widely used white lighting source, and its LE improves from 50 to 100 lm/W over the 60 years since its invention in 1938. Compared with Sunlight (standard white light), while the spectrum of incandescent light is continuous but insufficient in the blue and green range, fluorescent light emits more discretely, as shown on the light spectra distribution (Fig. 2). White-light sources based on reliable and energy-efficient LEDs have only been made available in recent decades through developments in semiconductors. Nowadays, current commercial white LEDs reach 150 lm/W, which is far higher than traditional incandescent light and fluorescent light. In terms of CRI, incandescent and halogen lights are capable of producing a white light of 100 CRI, but CRI value of fluorescent light is lowest ( $< 80$ ), while most white LEDs range between these two extremes (Fig. 1b). Since the full-width half-maximum (FWHM) of the QD emission spectrum is  $\sim 30\text{-}40\text{ nm}$ <sup>47, 48</sup>, compared with  $\sim 50\text{-}100\text{ nm}$  in inorganic phosphors<sup>49</sup>, QDs can be excellent luminescent sources for saturated emission colour and therefore higher CRI. Furthermore, old-generation white LEDs typically emit a cool bluish colour with high CCT ( $> 5000\text{ K}$ ) and low CRI (as seen in Fig. 1b) due to blue-chip and yellow phosphor combination and the lack of a narrow red-light component.<sup>3</sup> The narrow spectral emission of the QDs can offer more selective supplementary optical down-conversion to achieve efficient high CRI lighting source.

From a human health perspective, fluorescent light contains mercury, a neuro-toxin hazardous element, and it is difficult to recycle fluorescent light tubes. As can be noticed in Fig. 2, the spectrum of fluorescent light consists of a certain amount of ultraviolet (UV) light; the potential UV leakage can lead to user retina damage at close range or skin burn. The 100-120 hertz flickering may lead to eye fatigue and headache.<sup>50</sup> In general, there is increasing concern about the impact on the human circadian system from the blue light component in white lighting. Fluorescent and white LEDs emit more blue light than a sunset or an incandescent light. When people are subjected to these blue-rich white lighting source, photosensitive cells in the brain will be adversely influenced, which can have side effects such as sleep and waking cycles, metabolism, reproduction, mental alertness, blood pressure, heart rate, hormone production, and the immune system.<sup>41</sup> Consequently, it is of great importance to reduce the proportion of short-wavelength blue-light in general purpose white lighting and keep white light indirect, flicker-free and dimmable, suitably matching with the human circadian system. From the perspective of room lighting application, the large area panel lighting are much desired.<sup>1</sup>

#### **2.4 Working mechanism of WQLEDs**

There are two main approaches to realising WQLEDs. The first and mainstream approach combines blue or UV chips with a colour conversion layer consisting of phosphor and transparent polymer resin. The WQLEDs in this mode are usually

referred to as pc-WQLEDs and are physically based on PL behaviour of SSL materials. A typical configuration of a pc-WQLED involves a cerium-doped yttrium aluminium garnet (YAG: Ce<sup>3+</sup>) and a blue inorganic LED. As shown in Fig. 3a, some portion of emission from the blue LED excites a conversion phosphor to generate yellow emission, and when this emission is combined with the remaining portion of blue light, the human brain perceives white light, albeit with low CRI and CCT due to the missing red component.<sup>3, 51</sup> To address this issue, an extra red phosphor can be added but the emission spectra of conventional red phosphors are unfortunately too broad to avoid loss in LE. Alternatively, red/green/blue (R/G/B) conversion layers can be integrated simultaneously over a UV chip, where a full conversion occurs with all UV light absorbed and converted. (Fig. 3b)

The second approach is essentially the EL process in the luminescent QD materials, where white emission is generated by electron-hole pair recombination at the junctions formed within three primary-colour luminescent QD materials. The architecture of EL mode WQLEDs can be classified into three types according to the number of layers, namely, single-layer mixed, multi-layer and tandem structure (Fig. 3c). For the single mixed-QD WQLEDs, the emitting layer (EML) consists of a mixture of three R/G/B QD materials which are sandwiched between an electron-injecting cathode and a hole-injecting anode. A typical WQLED consists of (i) a front transparent electrode - e.g., indium tin oxide (ITO), (ii) electron/hole transport and hole/electron blocking layers, (iii) QD emitting layer, and (iv) a back electrode - e.g., Al or Au. In earlier times, blue emitting QDs were replaced with a blue-emitting molecule or polymer since high-performance blue QDs were difficult to fabricate.<sup>41, 52-55</sup> For multi-layered and tandem configuration WQLEDs R/G/B layers are coated subsequently, and different multiple transparent interconnecting layers (ICLs) are inserted between EMLs.

Internal quantum efficiency (IQE) and external quantum efficiency (EQE) are the main parameters used to quantitatively assess the quantum efficiency of WQLEDs. IQE is the efficiency of the charge recombination process inside the WQLEDs. EQE is defined as the ratio of the number of emitted photons to the number of injected electrons, and may be expressed as:

$$EQE = \eta_r \chi \eta_{PL} \eta_{oc}$$

where  $\eta_r$  is the fraction of injected charges that generate excitons in the QDs,  $\chi$  is the fraction of generated excitons in spin-allowed optical transitions and usually close to unity,  $\eta_{PL}$  is the PLQY for this optical transition and  $\eta_{oc}$  is the fraction of emitted photons that are coupled out of the WQLEDs. As WQLEDs often consist of solid-state phase QD films,  $\eta_{PL}$  directly limits the maximum device efficiency, which is associated with non-radiative Förster resonant energy transfer (FRET) of excitons to non-luminescent sites before non-radiative recombination,<sup>56-58</sup> non-radiative energy transfer to adjacent conducting layers<sup>59</sup>, injected-charge-induced Auger recombination and electric-field-induced exciton dissociation.<sup>60-62</sup>

### 3. Viable approaches for PL mode WQLEDs

Since the 1990s, the successful commercialisation of GaN blue-emitting LEDs has enabled WLEDs using SSL materials.<sup>63</sup> However, WLEDs based on blue-chip and YAG phosphor can only exhibit a yellowish-white colour, with CCT of 4000–8000 K, corresponding to the neutral and cool-white specification, and their CRI is typically lower than 80. However, in many applications such as indoor illumination, WLEDs are required to provide warm enough light with CCT > 4000 K and CRI higher than 80.<sup>38</sup>

64

The rapid development of solution-processed QDs exhibit great potential to be a better candidate for next-generation WLED phosphor materials.<sup>34, 65, 66</sup> Unlike conventional phosphor materials which might suffer from insufficient blue-light excitation and substantial scattering loss of light, the excitation and emission of QD materials can be easily shifted by changing size or composition.<sup>67</sup> The QD materials are sufficiently small to suppress light scattering and so high quantum efficiency and photostable QD materials are promising substitutes for conventional phosphors.

Early-stage research started from Cd-based QD materials because they feature excellent tunability relatively small overlap between emission and absorption spectra, and facile processability. In 2007, Nizamoglu *et al.* reported CdSe/ZnS core-shell WQLEDs. When QDs were single, binary, ternary and quaternary combined and then hybridized with InGaN/GaN LEDs, tristimulus coordinates (TCs), CCT and CRI parameters could be readily tuned.<sup>37</sup> Similarly, a blue/green two-wavelength InGaN/GaN LED coated with a red-emitting CdSe/ZnS QDs, and a blue InGaN/GaN LED with a single yellow-emitting CdSe/ZnSe QDs and a dual red and green-emitting CdSe/ZnSe have also been reported, with the latter achieving CIE coordinates of (0.33, 0.33) and CRI of 91.<sup>68</sup> Therefore, high colour rendering properties can be obtained by combining multiple-colour QDs as phosphor materials. Jang *et al.* fabricated WQLEDs via hybridizing Sr<sub>3</sub>SiO<sub>5</sub>: Ce<sup>3+</sup>, Li<sup>+</sup> phosphors and CdSe QDs on blue InGaN chips and their devices exhibited CRI of 90.1 and CCT of 8864 K.<sup>69</sup> Moreover, silica-coated InP/ZnS QDs together with green- and yellow-emitting phosphors have been successfully applied by Ziegler *et al.* in the fabrication of WQLEDs, allowing the prototype LED chips with 53 lm W<sup>-1</sup> luminous efficiency.<sup>70</sup>

CdSe/ZnS is the most studied core-shell QDs structure, but their significant lattice mismatch (ca. 12%) between CdSe and ZnS inevitably induces strain at the core-shell interface, which negatively affects both the PL efficiency and stability of CdSe/ZnS QD.<sup>71-73</sup> Likewise, InP/ZnS core-shell QDs, where a significant lattice mismatch of 7.7% between core and shell, possess a moderate quantum yield (QY).<sup>74</sup> To overcome this issue, an intermediate shell is usually introduced prior to an outer shell.<sup>75-77</sup> Apart from II-VI type semiconductor QDs, II-III-VI type, as Cd-free QDs, are also readily achievable through controlling the stoichiometry between group II, III, and VI ions or forming the solid solution between structurally similar phases, and is consequently

applied in WQLEDs. To date, Cu-III-VI QDs and their alloys with ZnS have been used in nearly all reports on WQLED applications, mainly due to two reasons. First, the emission of Cu-III-VI QDs can be tailored not only by size, but also by controlling the composition, defect type, and composite concentration, and by alloying with other elements such as Ga and Zn.<sup>32</sup> Second, Cu-III-VI QDs are characterised by a broad emission spectrum, which is negative for displays but beneficial to white lighting.<sup>78-82</sup> For example, Song *et al.* fabricated WQLEDs by using two combinations of ZnS coated Cu-In-Ga-S (CIGS) QDs and by optimising In/Ga ratio, reaching conversion efficiencies of 83%, CRI up to 78, and luminous efficacies up to 82.3 lm W<sup>-1</sup>.<sup>56</sup> Chen *et al.* combined red- and green-emitting CuInS (CIS)-based QDs within the same resin and the device reached a high CRI up to 95 and a luminous efficiency up to 70 lm W<sup>-1</sup>.<sup>83</sup>

Metal halide perovskite are emerging recently, which could be a suitable phosphor candidate.<sup>3-5</sup> However, to the best of our knowledge, there is still a lack of comprehensive studies on using perovskite QDs as phosphor materials for white lighting. Apart from some standard features of QD materials, metal halide perovskite QDs bear their unique properties such as long carrier lifetimes, high carrier mobility and high defect tolerance.<sup>84-88</sup> Indeed, in the WQLEDs, the halide perovskites could be used together with YAG phosphor, or replacing YAG, or to obtain R/G/B colours on UV LED, respectively.<sup>34</sup>

#### 4. Viable approaches for EL mode WQLEDs

##### 4.1 Cd-based WQLEDs.

In the early development stage, researchers used II-VI semiconductor QDs, such as CdSe, in combination with an emitting polymer to fabricate WQLEDs since CdSe QDs exhibit size-dependent colour tunability, high PLQY and good solution processability.<sup>89</sup> For example, Gigli *et al.* demonstrated hybrid organic/inorganic WQLEDs using blue-emitting poly[(9,9-dihexyloxyfluoren-2,7-diyl)-alt-co-(2-methoxy-5-{2-ethylhexyloxy}phenylene-1,4-diyl)] (PFH-MEH) polymer doped with red-emitting CdSe/ZnS core-shell structure QDs and Alq<sub>3</sub> small molecule. By accurately adjusting the concentration ratio of the QDs/PFH-MEH blend, authors successfully controlled the Förster energy and charge-transfer in devices and achieved the fabrication of relatively pure WQLEDs, with CIE coordinates at (0.30,0.33).<sup>93</sup> In 2006, the same research group realized the first hybrid WQLEDs with emission originating only from the R/G/B ternary CdSe/ZnS QDs.<sup>94</sup> The structure of WQLED and its control device are presented in Fig. 4a and 4b, wherein R-, G-, and B- CdSe/ZnS QDs are blended optimally with the (4,4',N,N'-diphenylcarbazole) (CBP) host, thereby obtaining the maximum brightness at 1050 cd m<sup>-2</sup> at 58 mA cm<sup>-2</sup> and turn-on voltage at 6 V in air. Additionally, according to the PL and EL spectra (Fig. 4d), it is claimed that the exciton generation on QDs happens *via* two mechanisms: I) direct charge injection and recombination on the ternary CdSe/ZnS QDs and II) Förster energy transfer from adjacent CBP and Alq<sub>3</sub> (Fig. 2c). But it should be noticed that this WQLED exhibited quite low current

efficiency (CE) at  $1.8 \text{ cd A}^{-1}$ , which is mainly because of low QY from QDs and insufficient charge injection from hole transport layer (HTL) and electron transport layer (ETL) layers.

Later on, a mixed-monolayer of R/G/B three colour emitting CdSe/ZnS WQLED was demonstrated, which can generate a broad spectral emission.<sup>27</sup> Although the fabricated device showed a CRI of 86 as compared to a 5500 K blackbody reference and CIE coordinates of (0.35, 0.41), its low EQE of 0.36% is unfavourable and far from the application requirement. To be more specific, compared with red and green CdSe/ZnS QDs, the performance of blue QDs is weaker due to their less efficient electron and hole injection and less probable exciton energy transfer from neighbouring polymer layers. As a result, blue QDs become the most challenging part in the mixed-monolayer WQLEDs for better performance. In 2015, Ki-Heon *et al.* reported the fabrication of multicolour-emissive WQLEDs *via* a solution-processing of ZnO NPs EHL and poly(9-vinylcarbazole) (PVK) EHL, which reached the record high EL performance such as the peak luminance values of  $23352 \text{ cd m}^{-2}$ , CE of  $21.8 \text{ cd A}^{-1}$ , and 10.9% EQE.<sup>28</sup>

In addition to mixing primary colour QDs in a single emitting layer, the multilayer WQLEDs *via* layer-by-layer deposition method can reduce inter-QD FRET with less contact between R/G/B different coloured QDs, thus better device performance can be expected. However, in the conventional deposition process (spin-coating, dip-coating, etc.), the previously coated QD layer will be damaged by subsequently miscible QDs layers. So, the traditional wet coating method would be incompatible with the sequential stacking of different coloured QD EMLs. How to avoid inhomogeneous QD films and fabricate a desirable morphology between QD layers became one of the main concerns for multi-layered WQLEDs. In this regard, novel methods have been proposed for the formation of multi-layered QD EMLs. For instance, Bae *et al.* introduced a layer-by-layer way by using electrostatic interactions between each QD layer *via* the sequential deposition of oppositely charged green and red QDs.<sup>95</sup> Besides, polydimethylsiloxane (PDMS) stamp-based dry transfer printing has been used for the realization of R/G/B QD full-colour display devices.<sup>39, 96</sup> However, the transfer printed WQLEDs inevitably result in spectra overlap, which means that the device would not possess highly colour-pure R/G/B constituents. Moreover, the WQLEDs, as mentioned above only exhibit a mediocre performance in terms of luminance and CE<sup>39, 96</sup>

Recently, Yang *et al.* reported all-solution-processed R/G/B full-colour WQLEDs with a standard structure, where sequentially coated R/G/B QD EMLs were sandwiched by PVK and ZnO NPs (Fig. 5a and 5c).<sup>97</sup> The creative point is that an ultrathin ZnO NP buffer layer was inserted between different-coloured QD EMLs, so that the underlying QD layer was protected from the subsequent solution coating process. (As PL results presented in Fig. 5b (i) and (ii), where hexane rinsing test proved.) Even though Fig. 5d (i) shows the three primary colour emission spectra were well-separated with marginal overlap, the emission colour of as-obtained WQLEDs was still unstable as emission intensities increased dissimilarly with rising voltage (Fig. 5d (ii)). Some previous

studies also presented similar voltage-dependent spectral variance, and the smaller bandgap QDs would generally contribute less EL when devices are biased at higher working voltage.<sup>28, 98, 99</sup> Specifically, as shown in energy band diagram within multi-layered WQLED, the electron injection barrier from ETL to red QD is much lower than the hole injection barrier from HTL to blue QD. Then the exciton formation zone can be at the blue QD EML. But under higher voltage bias, HTL-to-blue QD hole injection becomes sufficient, leading to exciton generation across the whole QD EMLs and marginally changed luminance, CE and EQE. (Fig .5f)

Consequently, it is still challenging to avoid migration of the exciton recombination zone inside multi-layered WQLEDs, which hinders further improvement of WQLED performance matching the over 20% state-of-the-art monochromatic QLEDs.<sup>26, 100-102</sup> As mentioned above, adoption of the inserted ZnO layer in multi-layered WQLEDs will potentially bring about following problems: 1) As an ETL material, ZnO would prevent sufficient hole injection between QD EMLs and thus further impair balanced charge injection process, especially hole injection from B-QDs to G/R-QDs; 2) adoption of the ZnO layer could also introduce defects which may quench excitons and adversely affect the device performance; 3) ~ 3nm ZnO cannot entirely suppress intrinsic inter-QD FRET. Other architectures should be applied to realize higher current efficiency, purer colour emission and more stable WQLEDs for efficient lighting and backlight applications.

Tandem architectures have been broadly applied in the manufacture of white organic light-emitting diodes (WOLEDs) in industry because tandem WOLEDs have proved their excellent function, stable performance and long lifetime in applications such as OLED TV and OLED lighting panels.<sup>103-105</sup> This development experience has been brought into the fabrication of tandem WQLEDs. Typically, in a tandem device, two or more EL units are serially connected through a transparent ICL thus the CE and EQE of tandem LEDs are usually two or more times higher than those of the single LEDs as current passes through more than one EL layers. However, there are still barriers preventing the development of tandem WQLEDs. First, QD EMLs are usually deposited by solution-processing, whereas most efficient small molecule ICLs can be easily washed away by the solvents when QDs are subsequently coated. Second, it is challenging to maintain every homogeneous layer in good condition because the tandem structure contains more functional layers than any others. This is even more challenging with WQLEDs due to the requirement of successive deposition of R/G/B three layers. Therefore, to date, all-solution-processed tandem WQLEDs have seldom been reported.

In 2017, Zhang *et al.* first achieved a white tandem WQLED by serially connecting R/G/B CdZnSeS/ZnS QDs EMLs using a proposed ZnMgO/ (poly(3,4-ethylenedioxythio-phenylene):poly(styrene sulfonate))(PEDOT: PSS) heterojunction ICL.<sup>98</sup> Unfortunately, the resultant WQLEDs exhibited a low CE of 4.75 cd A<sup>-1</sup> and a CIE coordinate of (0.30, 0.44), which can be attributed to morphology deterioration

between pre-deposited ZnMgO and post-deposited PEDOT: PSS associated with their hydrophilicity mismatch. Replacing hydrophilic PEDOT: PSS with other hydrophobic ICL materials or adjusting hydrophilicity by interface engineering could be one solution to this problem.

By replacing the aqueous PEDOT: PSS with PMA (polyoxometalate phosphomolybdic acid), Cao *et al.* reported tandem WQLEDs with a high CE of  $60.4 \text{ cd A}^{-1}$  and EQE of 27.3% at a luminance of  $100000 \text{ cd m}^2$ .<sup>106</sup> The device architecture is presented in Fig. 6a, as well as a cross-sectional STEM image in Fig. 6b. Fig. 6d gives the energy level diagram of this tandem WQLED and the energy level diagram of red QDs/ZnO/PMA/HTL/red QDs is shown in Fig. 6e, which explains the charge formation and injection within heterointerface between neighbouring QD EMLs. To be more precise, when a device is under forward bias, the shifting of the vacuum level will lead to smooth electron transfer from the conduction band (CB) of PMA to that of ZnO before injection into CB of the QD EML. In contrast, the hole on the highest occupied molecular orbital (HOMO) of the HTL transfers in the opposite direction to the valence band (VB) of the other adjacent QD EML.<sup>107, 108</sup> Consequently, each layer of R/G/B EMLs are spatially separate, and FRET is thus effectively prohibited in the tandem WQLEDs. Even when driving bias varies, the recombination zone in tandem WQLEDs will not migrate owing to inserted ICLs. Therefore, WQLEDs naturally exhibit a comparable level of efficiency with that of the latest monochromatic QLEDs, which is far better than mixed-QD and multi-layered WQLEDs mentioned above.

## 4.2 InP WLEDs

Despite apparent advantages such as high PLQY, narrow emission linewidth and excellent photostability of Cd-based QDs,<sup>109-111</sup> the inherent toxicity of cadmium makes it environmentally restricted and its broad commercialisation is thus doubted in both academia and the public.<sup>112</sup> InP with a bandgap of 1.35 eV has been considered as one of the potential alternatives to Cd-based QDs because it can provide comparable emission wavelength but without the toxicity problem.<sup>113-115</sup>

Similar to Cd-based WQLEDs, in the initial period, InP-based WQLEDs were first realized by integration of green InP QDs with R/B emissive polymers. In 2012, research by Sun *et al.* demonstrated a hybrid WQLED based on one-pot solvothermal synthesised InP/ZnS core-shell QDs sandwiched by Poly(N, N'-bis-4-butylphenyl-N,N'-bisphenyl)benzidine (Poly-TPD) and 2,2',2''-(1,3,5-Benzinetriyl)-tris(1-phenyl-1-H-benzimidazole) (TPBi), which exhibited a high CRI of 91 (Fig. 7a and 7b).<sup>29</sup> Then, the same research group reported another InP-based WQLEDs with the same device architecture but higher CRI of 95 and better CIE coordinates of (0.349, 0.342).<sup>116</sup> Analogous to multi-layered Cd-based WQLEDs, ternary combination InP-based WQLEDs also exhibited a distinctive voltage dependence since EL spectra, and CIE chromaticity coordinates of WQLEDs shifted as a function of bias (Fig. 7c and 7d). Meanwhile, there has been some development of monochromatic InP QLEDs,<sup>117-120</sup> but colour purity and emission spectrum tunability are still much inferior to the well-

developed Cd-based QDs. The inferior properties stem from the strong coordinating strength of indium ligands and hard core-shell formation which induce difficulties in synthesis procedure, especially in the case of blue light-emitting InP QDs. As a result, high-performance fully colloidal InP QD-based WLEDs are rarely reported.

### 4.3 CIGS WQLEDs

Cu chalcogenide QDs are also good candidates to replace toxic heavy-metal (Cd and Pb) compound semiconductors in solution-processed WQLEDs. Among the broad variety of Cu chalcogenide QDs, Cu (In, Ga)(S, Se)<sub>2</sub> (CIGS/CIGSe) QDs and their alloys with ZnS have been used as the EL material in many Cu-based WQLEDs.<sup>121-123</sup> The emission wavelength of CIGS QDs can be easily controlled by varying the composition,<sup>122-125</sup> which enables not only high colour gamut and broad PL emission to achieve high CRI but also relatively long lifetimes in WQLEDs.<sup>32</sup> For example, WQLEDs were obtained by Zhang *et al.* using red-emitting ZnCuInS/ZnS core/shell QDs and the blue-green emission of Poly-TPD in a bilayer structure, whose CRI reaching up to 92 as compared to 5310 K blackbody reference (Fig. 8a and 8b).<sup>126</sup> Recently, Teng *et al.* fabricated WQLEDs by using yellow Cu-In-Zn-S/ZnS core/shell QDs blended with Poly(9,9-dioctylfluorene-alt-N-(4-sec-butylphenyl)-diphenylamine) (TFB), whose EL colour were reported to be tunable from blue-green to white by varying the thermal annealing temperatures.<sup>127</sup> The resultant WQLEDs exhibited a low turn-on voltage of 2.5 V and a maximum luminance of 1500 cd m<sup>-2</sup>, with a CRI of 90 and CIE coordinates of (0.33, 0.32).

As mentioned above, CIGS QDs naturally tend to have a broad PL emission, and this will be disadvantageous in the fabrication of monochromatic QLEDs, which means reports focus on multi-layered and tandem CIGS-based WQLEDs. In this sense, use of a single QD emitter rather than multiple ones as EML may be highly advantageous for CIGS-based WQLEDs, by either doping impurity ions such as Cu<sup>+</sup> and Mn<sup>2+</sup> into QD host,<sup>128</sup> or introducing radiative charge recombination at defect-associated intragap states in QDs.<sup>129, 130</sup> In 2016, Yang *et al.* obtained a high, broad visible coverage emission CGS/ZnS QDs with the highest QY of 76% by optimally controlling the off-stoichiometry of Cu/Ga and adjusting the ZnS-shelling period of Cu/Ga.<sup>30</sup> In this WQLED, a very stable white-light emission can be maintained regardless of the change of bias voltage, whose emission is attributed solely to the radiative recombination of the injected charged QD EML, instead of including any contribution from HTL emission (Fig. 8c to 8g).

### 4.4 Perovskite WQLEDs

Hybrid organic-inorganic and all-inorganic metal halide perovskite QDs (HOIP and AIP QDs) have been intensively studied during the past few years.<sup>35, 131, 132</sup> The first known halide perovskite was based on organic cations, featuring small exciton binding energy, strong absorption and high carrier mobility, and therefore proved successful in photovoltaic (PV) devices.<sup>85, 133, 134</sup> Apart from PV devices, perovskite materials have also shown their superb properties when they were applied in other optoelectronic

devices, including display, WLEDs and others.<sup>135-138</sup> The first breakthrough of perovskite-based LEDs was a MAPbBr<sub>3</sub> green LED reported in 2014, which exhibited a bright luminance of 364 cd m<sup>-2</sup> and EQE of 0.1% at room temperature.<sup>139</sup> Only one year later, by elaborately interfacial engineering, MAPbBr<sub>3</sub>-based monochromatic LEDs have achieved a 20-fold enhancement in LE and outstanding improvement in terms of luminance and EQE, reaching 20000 cd m<sup>-2</sup> and 3.5%, respectively.<sup>140</sup> It should be pointed out that despite remarkable progress in green- and red- perovskite-based LEDs, the efficiency of blue perovskite-based QLEDs has not reached a comparable level, which reasonably hampers fabrication of HOIP-based WQLEDs where desired R/G/B HOIP QDs are prerequisites.

In 2015, the first fabrication of CsPbX<sub>3</sub>-based AIP QLEDs was reported by Song *et al.* with the structure of ITO/PEDOT: PSS/PVK/QDs/TPBi/LiF/Al (Fig. 9a).<sup>141</sup> Noticeably, the colour of devices can be adjusted from blue to green and orange by changing the content and anion category, which achieved luminances of 742 cd m<sup>-2</sup>, 946 cd m<sup>-2</sup>, and 528 cd m<sup>-2</sup>, with external quantum efficiencies of 0.07%, 0.12%, and 0.09%, respectively. As seen in Fig. 9b and 9c, the FWHM was smaller than 30 nm for all colours, and three colour QLEDs can cover the upper left part of the CIE diagram.

For both HOIP and AIP QDs, applications in WQLEDs are rarely reported. For instance, Yang *et al.* synthesized CsPbBr<sub>x</sub>Cl<sub>3-x</sub> QDs, with a blue emission peak at 470 nm and with narrow bandwidth.<sup>142</sup> The authors then demonstrated WQLEDs by blending blue-emitting CsPbBr<sub>x</sub>Cl<sub>3-x</sub> QDs with orange-emitting polymer, poly[2-methoxy-5-(2-ethylhexyloxy)-1,4-phenylenevinylene](MEH: PPV) as EML (Fig. 9d). Within active EML, Dexter energy-transfer and Förster energy transfer were verified to coincide, allowing the device to reach a brightness of 350 cd m<sup>-2</sup> and CIE chromaticity coordinate at (0.33,0.34) (Fig. 9e and 9f). Nevertheless, only at a high driving bias of 8V can the ultimate light be emitted, and an ideal CIE coordinate reached, indicating a reduction of turn-on voltage is required for better performance. Blending two types of perovskite materials is another method for perovskite-based WQLEDs fabrication. Mao *et al.* demonstrated an all-perovskite WQLED with stacking of two-dimensional red-emitting (CH<sub>3</sub>CH<sub>2</sub>CH<sub>2</sub>NH<sub>3</sub>)<sub>2</sub>CsPb<sub>2</sub>I<sub>7</sub> perovskite and cyan colour CsPb(Br, Cl)<sub>3</sub> QDs as EMLs.<sup>143</sup> By carefully choosing the mixture of bis(1-phenyl-1H-benzo[d]imidazole)-phenylphosphine oxide (BIPO) and Poly-TPD as ICL, the device not only exhibited CIE coordinates of (0.32, 0.32) and CCT of 6000 K, but also maintained steady CIE coordinates in a wide range of driving current density from 2.94 to 56.29 mA cm<sup>-2</sup>. Despite satisfying device performance obtained in recent years, the stability of HOIP and AIP QDs WLEDs remains a significant issue in this early stage materials platform.<sup>144</sup> It has gradually become clear that perovskites lack structural and chemical stability in the presence of moisture or heat. Phase segregation, ion migration and some electrochemical reactions also account for degradation of perovskite materials in optoelectronic devices.<sup>145-147</sup>

To sum up, the Cd-based WQLEDs exhibit exceptional and stable device performance,

with tandem WQLEDs reaching a high CE of 60.4 cd A<sup>-1</sup> and EQE of 27.3% at a luminance of 100000 cd m<sup>2</sup>.<sup>106</sup> Nevertheless, the heavy-metal property of Cd-based QDs prevent their widespread application in general white-lighting scenarios due to public health and environmental concerns. InP and CIGS are emerging as promising alternative nanocrystals for WQLEDs as their nontoxicity and partially abundant composition. However, the emission linewidth of the typical InP QDs reported is wider (50–80 nm) than that of CdSe (15–40 nm), which leads to a worse colour purity compared to CdSe.<sup>29, 148</sup> CIGS QDs, on the other hand, may encounter more challenges because the control of these quaternary composition QD surface stoichiometry/defects and assembly/deposition/combination during synthesis stage is rather complicated, in particular, a comprehensive understanding and theoretical models for the origin of PL broadness, and composition-dependent emission wavelength and PLQY is still lacking.<sup>32</sup> As for perovskite-based WQLEDs, it is easier to achieve higher PLQY, narrower emission linewidth compared to Cd-based, InP and CIGS QDs; but the perovskite stability and corresponding device lifetime is required to be further improved.

## **5 Outlook and opportunities for future hybrid WQLEDs**

As highlighted in this review, there has been a rapid development of WQLEDs over the past decade. The intensive research on QD material properties and application in lighting has continuously produced breakthroughs beyond the state-of-the-art SSL in terms of colour purity, device efficiency and versatility.

### **5.1 PL mode hybrid WQLEDs**

The WQLEDs based on PL mode mainly rely on the adoption of novel QD-based phosphor materials since InGaN/GaN blue-chip has already been commercialised. The main challenge for PL mode WQLEDs lies on new methods to achieve CCT > 4000 K and CRI higher than 80. However, improving the photostability and reducing the thermal quenching is supposed to be another challenge since PL mode LEDs generally work at high flux and temperature (>100 W cm<sup>-2</sup> 150°C) and QD materials may be unstable under long operation time under these conditions.<sup>33</sup> Cores of QDs are usually passivated with shells to improve QD photostability and thermal stability since pure cores may not maintain long-term stability in solution and suffer from photo-oxidation.<sup>149-151</sup> For example, ZnS is an ideal outer shell material for QD materials as it shows better photo-oxidation resistance to CdSe QDs than CdS shell under continuous UV irradiation, which is attributed to the larger bandgap difference between CdSe and ZnS, lowering the photogenerated charge carrier density.<sup>152</sup> Therefore, optimal design of strain-graded core/shell interfaces, alloyed QDs or gradient composition shells structure could be solutions to photostability and thermal quenching problems in PL mode hybrid WQLEDs. Remoted type WLEDs may provide an alternative way to solve the stability issues; however, more work should be done to approach the industrial requirements.<sup>49</sup>

### **5.2 EL mode hybrid WQLEDs**

In terms of EL mode WQLEDs, considerable progress has been achieved in both QD materials and device architectures. The early-stage EL mode WQLEDs are mainly based on the development of Cd-based QD WLEDs. Work has progressed from mixed-QD single emission layer to the stacking of R/G/B multi-layered and then to a tandem structure where inter-connecting transfer layers have been inserted. At present, the performance of Cd-based WLEDs has reached the same level as the latest WOLEDs.<sup>103-105</sup> However, even though embedded charge transport layers can suppress non-radiative Auger recombination and FRET between adjacent EMLs and avoid intermixing problems, the balance of hole and electron transport will inevitably be another issue to be confronted. Moreover, for tandem Cd-based WQLEDs, how to develop a novel fabrication process and at the same time maintain balanced charge carrier injection are remaining challenges to be investigated in future studies.

Meanwhile, heavy-metal-free environmental-friendly WQLEDs has become a new research trend. Currently, the device performance of InP and Cu chalcogenide-based WQLEDs is far below the requirement of practical applications, and it is mandatory to improve their red- and green- QLEDs to catch up with Cd-based counterparts before realising full-colour WQLEDs.<sup>74</sup> As for InP and CIGS blue-emitting QLEDs, it is difficult to efficiently inject carriers into blue QDs due to their wide bandgap, corresponding with energy transfer in the QD films, interface charge transfer between blue QDs and CTLs, and electric field-induced quenching in blue QLEDs. It is also hard to achieve high efficiency and sharp and narrow PL intensity in ternary and quadruple Cu chalcogenide-based blue-emitting QDs. However, the broad PL emission and relatively long lifetimes may represent a disadvantage in monochromatic LEDs, but it is an advantage to secure a high-colour CRI in WQLEDs.

The PLQYs for perovskite QDs are approaching nearly 100% in both solutions and solids, rendering desirable device efficiencies.<sup>153-155</sup> However, blue-emitting Perovskite-based LED devices remain low efficiency, which might be related to poor electrochemical stability and low PLQY. This can be attributed to surface defects that inherently induce the nonradiative electron-hole recombination. Given the physical and chemical nature of perovskite-based QD materials, their stability against moisture, heat, oxygen, and electric field will continue to be an area of intense research. The lack of data about the device stability and the degradation mechanism of the WQLEDs – i.e., loss of efficiency and colour changes (CRI, CCT, *etc.*)- complicates the path through new achievements toward highly stable Perovskite-based WQLEDs.

Table 1. Summary of selected high-performance WQLEDs fabricated from various QD combination

QD composition	Device architecture	x/y CIE	CCT (K)	CRI	LE (lm W <sup>-1</sup> )	CE (cd A <sup>-1</sup> )	EQE (%)	Mode	Ref.
InP/ZnS	InGaN//YAG:Ge//Sr <sub>0.94</sub> Al <sub>2</sub> O <sub>4</sub> :Eu <sub>0.06</sub> //InP/ZnS-silicone	-	3200 - 6500	86	53	-	-	PL	<sup>69</sup>
CdSe	InGaN//Sr <sub>3</sub> SiO <sub>5</sub> :Ce <sup>3+</sup> ,Li <sup>+</sup> //CdSe	-	8864	90.1	14	-	-	PL	<sup>70</sup>
CIGS/ZnS	InGaN//GIGS/ZnS-silicone	-	-	78	82.3	-	-	PL	<sup>56</sup>
CuInS <sub>2</sub>	InGaN//CuInS <sub>2</sub> -silicone	0.312/0.303	6832	90.5	30	-	-	PL	<sup>83</sup>
CdSe/ZnS	ITO//PEDOT:PSS//PFH-MEH: CdSe/ZnS//Alq <sub>3</sub> //Ca/Al	0.30/0.33	-	-	-	-	-	EL	<sup>93</sup>
CdSe/ZnS	ITO//PEDOT:PSS//CBP: CdSe/ZnS//Alq <sub>3</sub> //Ca/Al	0.32/0.45	-	-	-	2.2	-	EL	<sup>94</sup>
CdSe/ZnS	ITO//PEDOT:PSS//TPD//CdSe/ZnS//TAZ//Alq <sub>3</sub> //Mg/Ag	0.35/0.41	5500	86	-	-	0.36	EL	<sup>27</sup>
CdSeS/ZnS(R), CdZnSeS/ ZnS(G), CdZnS/ZnS(B),	ITO//PEDOT:PSS//PVK//Mixed RGB QDs//ZnO//Al	-	-	-	-	21.8	10.9	EL	<sup>28</sup>
CdSe/CdS/ ZnS(R), CdSe/ZnS (G,B)	ITO//PEDOT:PSS//TFB//CdSe/ZnS(patterned)//ZnO//LiF/Al	0.39/0.38	-	-	-	-	2.35	EL	<sup>96</sup>
CdSeS/ZnS(R), CdZnSeS/ ZnS(G), CdZnS/ZnS(B)	ITO//PEDOT:PSS//PVK//QDs(B)/ZnO/QDs(G)/ZnO/QDs(R)/ZnO//Al	0.32/0.33	-	-	-	15.9	6.8	EL	<sup>97</sup>

CdZnSe/CdS/ZnS(R), CdZnSeS/ZnS(G), ZnCdS/ZnS(B)	ITO//PEDOT:PSS//PVK//QDs(R)//ZnMgO//PEDOT:PS//PVK//QDs(G)//ZnMgO//PEDOT:PSS//PVK//QDs(B)//ZnMgO//Al	0.36/0.44	-	-	-	4.75	2.0	EL	98
CdSe/ZnS(R,G), ZnCdS/ZnS(B)	ITO//PEDOT:PSS//TFB//QDs(B)//ZnO//PMA//TFB//QDs(G)//ZnO//PMA//TFB//QDs(R)//ZnO//Ag	0.405/0.388	-	-	10.55	60.4	27.3	EL	106
InP/ZnS	ITO//PEDOT:PSS//Poly-TPD//InP/ZnS//TPBi//LiF/Al	0.332/0.338	-	91	-	-	-	EL	29
InP/ZnSeS	ITO//PEDOT:PSS//Poly-TPD//InP/ZnSeS//TPBi//LiF/Al	0.349/0.342	4710	95	-	-	-	EL	116
ZnCuInS/ZnS	ITO//PEDOT:PSS//Poly-TPD//ZnCuInS/ZnS//Al	0.336/0.339	5310	92	-	-	-	EL	126
CuInZnS/ZnS	ITO//PEDOT:PSS//TFB//TFB:QDs//ZnO//Al	0.33/0.32	-	90	-	0.13	-	EL	127
CGS/ZnS	ITO//PEDOT:PSS//PVK//CGS/ZnS//ZnO//Al	0.294/0.334	-	88	1.9	3.6	1.9	EL	30
CsPbBr <sub>x</sub> C <sub>l<sub>3-x</sub></sub>	ITO//NiO <sub>x</sub> //MEH:PPV:CsPbBr <sub>x</sub> Cl <sub>3-x</sub> //TPBi//LiF/Al	0.33/0.34	-	-	-	-	-	EL	142
PA <sub>2</sub> CsPb <sub>2</sub> I <sub>7</sub> (R), Poly-TPD(G), CsPb(Br, Cl) <sub>3</sub> (B)	ITO//PEDOT:PSS//PA <sub>2</sub> CsPb <sub>2</sub> I <sub>7</sub> //BIPO:PolyTPD//CsPb(Br,Cl) <sub>3</sub> //TPBi//LiF/Al	0.32/0.32	6000	-	-	-	-	EL	143

### 5.3 Future opportunities for hybrid QDs WQLEDs

The field of WQLED has made tremendous strides, and the need for lower cost, higher efficiency devices will continue to drive materials and device innovation. While WQLEDs incorporating Cd-free QDs have been demonstrated, much of understanding of WQLEDs EL-mode performance is linked to Cd-containing QDs. While the percentage of heavy metals in WQLEDs can be small, demonstration of high-

performing Cd-free EL-mode WQLEDs will likely be the future focus because they are crucial to securing widespread industry and government support for ambient lighting. As the colloidal QDs based LEDs have been successfully commercialised in high-definition television (HDTV), it will become possible for WQLEDs to build their market share in global ambient lighting applications.

*In terms of device structure opportunities*, the most pertinent investigations for improving WQLEDs performance should be comparative studies that seek to determine white colour hybridization pathways of making high-performance tandem structure. For instance, while perovskite-based QD can provide very high colour purity luminescence with FWHM around 20 nm, CIGS-based QDs usually generate broad PL emission, which means by hybridization of green and blue perovskite-based QDs with red CIGS-based QDs, it is possible to accomplish successful colour rendition of illumination together with an excellent spectral overlap between the responsivity of the human eye and the emission spectrum of the WQLED. Additionally, high quantum efficiency blue-emitting multi-shelled InP-based and ZnSeTe QDs have recently enabled high-performance blue QLEDs, which can be alternative to current low-efficiency perovskite-based and CIGS-based blue QDs and thus applied in tandem WQLEDs.<sup>120, 156, 157</sup> Furthermore, CIGS-based QDs are more air- and moisture-stable than perovskite-based QDs and InP-based QDs. Therefore, covering blue and green all-inorganic perovskite-based QDs or InP-based QDs with red-emitting CIGS-based QDs in tandem may be a solution to the realisation of high CRI, proper CCT, high LE and long-time operation WQLEDs. Meanwhile, the optimized InP/ZnSe/ZnS and carbon dots are also able to generate impressive EQE; therefore, these two types of QD materials can also be blue-emitting layers in the tandem structure.<sup>31, 158</sup>

*In terms of materials opportunities*, 'single particle' type white QDs, including alloyed CIGS-based, carbon dot-based, and perovskite-based QDs can be regarded as a most promising approach for WQLED material innovation. These 'single particle' type WQLEDs have outstanding advantages for subsequent device fabrication since only one white emitting QD layer involved in the final device structure which excludes multiple colour layer deposition, phase separation, emission quenching, and colour instability issues.<sup>131, 159, 160</sup> In addition, two-dimensional (2D) materials including carbon nanosheets, graphene nanosheet and transition metal dichalcogenides (TMDC), exhibit strong emission covering the whole visible spectrum and therefore become potential white QDs or hybrid white emitter materials for WQLEDs.<sup>161-169</sup> Although the electrical control of circularly polarized light emission in TMDC LEDs has been theoretically and experimentally reported, there are still several ongoing challenges to practical device application such as room temperature EL polarization and mechanisms for electrically controlling circularly polarized light emission. Based on these emerging 'single particle' white QDs and 2D materials, it might also be possible to construct double-heterostructure LEDs by sandwiching the white QDs between two large-bandgap TMDCs with opposite doping polarity, allowing for the confinement of light and carriers simultaneously. Given the large variety of available 2D materials and white

QDs in combining them, these heterostructures may not only compete as light emitters in the visible spectral SSL, but they could also trigger the development of applications in less explored large-area flexible ambient lighting.

### **Author contributions**

B. H. conceived the idea and led the preparation of the manuscript with the input from all co-authors.

### **Conflicts of interest**

There are no conflicts to declare.

### **Acknowledgements**

M.L. would like to thank the financial support from the Science and Technology Foundation of Henan Province (No. 192102210044). J.I.S. thank the NRF grant funded by the Korea government (MSIT) (2019R1A2C1007883), and Basic Science Research Program through the NRF funded by the Ministry of Education (2016R1A6A1A03012877). I.K.P. would like to acknowledge the financial support from the Basic Science Research Program through the National Research Foundation of Korea (NRF) funded by the Ministry of Science and ICT (NRF2018R1A2B6006968). B.H. would like to acknowledge the financial support by the Cardiff University.



Dr Bo Hou is a Lecturer at the School of Physics and Astronomy, Cardiff University. He obtained his PhD in physical chemistry from the University of Bristol in earlier 2014, where he studied the semiconductor photo-electrochemistry and microstructure analysis of colloidal QDs. He then worked as a postdoctoral research assistant at the University of Oxford (2014-2018), and a Senior Research Fellow at the University of Cambridge (2018-2020). His research interests include QD synthesis, QD optoelectronics, electron microscopy (TEM) and dynamic charge transfer analysis.

## References:

1. S. Reineke, *Nature Materials* **14** (5), 459-462 (2015).
2. Q. Dai, C. E. Duty and M. Z. Hu, *Small* **6** (15), 1577-1588 (2010).
3. N. K. Kumawat, Z. Yuan, S. Bai and F. Gao, *Israel Journal of Chemistry* **59** (8), 695-707 (2019).
4. Y. Zhao, J. Li, Y. Dong and J. Song, *Israel Journal of Chemistry* **59** (8), 649-660 (2019).
5. B. Hou, *Israel Journal of Chemistry* **59** (8), 637-638 (2019).
6. H. Zhong and Y. Wang, *Nature Photonics* **14** (2), 65-66 (2020).
7. B. Hou, M. Sohn, Y.-W. Lee, J. Zhang, J. I. Sohn, H. Kim, S. Cha and J. M. Kim, *Nano Energy* **62**, 764-771 (2019).
8. J. M. Caruge, J. E. Halpert, V. Wood, V. Bulović and M. G. Bawendi, *Nature Photonics* **2** (4), 247-250 (2008).
9. K.-S. Cho, E. K. Lee, W.-J. Joo, E. Jang, T.-H. Kim, S. J. Lee, S.-J. Kwon, J. Y. Han, B.-K. Kim, B. L. Choi and J. M. Kim, *Nature Photonics* **3** (6), 341-345 (2009).
10. B. S. Mashford, M. Stevenson, Z. Popovic, C. Hamilton, Z. Zhou, C. Breen, J. Steckel, V. Bulovic, M. Bawendi, S. Coe-Sullivan and P. T. Kazlas, *Nature Photonics* **7** (5), 407-412 (2013).
11. V. Adinolfi and E. H. Sargent, *Nature* **542** (7641), 324-327 (2017).
12. F. P. García de Arquer, A. Armin, P. Meredith and E. H. Sargent, *Nature Reviews Materials* **2** (3), 16100 (2017).
13. B. Hou, Y. Cho, B. S. Kim, J. Hong, J. B. Park, S. J. Ahn, J. I. Sohn, S. Cha and J. M. Kim, *ACS Energy Letters* **1** (4), 834-839 (2016).
14. G. H. Carey, A. L. Abdelhady, Z. Ning, S. M. Thon, O. M. Bakr and E. H. Sargent, *Chemical Reviews* **115** (23), 12732-12763 (2015).
15. D. Kufer and G. Konstantatos, *ACS Photonics* **3** (12), 2197-2210 (2016).
16. J. Y. Kim, O. Voznyy, D. Zhitomirsky and E. H. Sargent, *Advanced Materials* **25** (36), 4986-5010 (2013).
17. R. Saran and R. J. Curry, *Nature Photonics* **10** (2), 81-92 (2016).
18. E. J. Gansen, M. A. Rowe, M. B. Greene, D. Rosenberg, T. E. Harvey, M. Y. Su, R. H. Hadfield, S. W. Nam and R. P. Mirin, *Nature Photonics* **1** (10), 585-588 (2007).
19. F. Hetsch, N. Zhao, S. V. Kershaw and A. L. Rogach, *Materials Today* **16** (9), 312-325 (2013).
20. Y. Jiang, S.-Y. Cho and M. Shim, *Journal of Materials Chemistry C* **6** (11), 2618-2634 (2018).
21. W. K. Bae, Y.-S. Park, J. Lim, D. Lee, L. A. Padilha, H. McDaniel, I. Robel, C. Lee, J. M. Pietryga and V. I. Klimov, *Nature Communications* **4** (1), 2661 (2013).
22. Y. Yang, Y. Zheng, W. Cao, A. Titov, J. Hyvonen, J. R. Manders, J. Xue, P. H. Holloway and L. Qian, *Nature Photonics* **9** (4), 259-266 (2015).
23. Q. Sun, Y. A. Wang, L. S. Li, D. Wang, T. Zhu, J. Xu, C. Yang and Y. Li, *Nature Photonics* **1** (12), 717-722 (2007).
24. L. Qian, Y. Zheng, J. Xue and P. H. Holloway, *Nature Photonics* **5** (9), 543-548 (2011).

25. S. Nam, N. Oh, Y. Zhai and M. Shim, *ACS Nano* **9** (1), 878-885 (2015).
26. X. Dai, Z. Zhang, Y. Jin, Y. Niu, H. Cao, X. Liang, L. Chen, J. Wang and X. Peng, *Nature* **515** (7525), 96-99 (2014).
27. P. O. Anikeeva, J. E. Halpert, M. G. Bawendi and V. Bulović, *Nano Letters* **7** (8), 2196-2200 (2007).
28. K.-H. Lee, C.-Y. Han, H.-D. Kang, H. Ko, C. Lee, J. Lee, N. Myoung, S.-Y. Yim and H. Yang, *ACS Nano* **9** (11), 10941-10949 (2015).
29. X. Yang, D. Zhao, K. S. Leck, S. T. Tan, Y. X. Tang, J. Zhao, H. V. Demir and X. W. Sun, *Advanced Materials* **24** (30), 4180-4185 (2012).
30. J.-H. Kim, D.-Y. Jo, K.-H. Lee, E.-P. Jang, C.-Y. Han, J.-H. Jo and H. Yang, *Advanced Materials* **28** (25), 5093-5098 (2016).
31. Y.-H. Won, O. Cho, T. Kim, D.-Y. Chung, T. Kim, H. Chung, H. Jang, J. Lee, D. Kim and E. Jang, *Nature* **575** (7784), 634-638 (2019).
32. C. Coughlan, M. Ibanez, O. Dobrozhan, A. Singh, A. Cabot and K. M. Ryan, *Chem Rev* **117** (9), 5865-6109 (2017).
33. J. McKittrick and L. E. Shea-Rohwer, *Journal of the American Ceramic Society* **97** (5), 1327-1352 (2014).
34. T. Guner and M. M. Demir, *physica status solidi (a)* **215** (13) (2018).
35. Y. Wei, Z. Cheng and J. Lin, *Chem Soc Rev* **48** (1), 310-350 (2019).
36. F. Yan, S. T. Tan, X. Li and H. V. Demir, *Small* **15** (47), 1902079 (2019).
37. S. Nizamoglu, T. Ozel, E. Sari and H. V. Demir, *Nanotechnology* **18** (6), 065709 (2007).
38. S. Nizamoglu, G. Zengin and H. V. Demir, *Applied Physics Letters* **92** (3), 031102 (2008).
39. T.-H. Kim, K.-S. Cho, E. K. Lee, S. J. Lee, J. Chae, J. W. Kim, D. H. Kim, J.-Y. Kwon, G. Amaratunga, S. Y. Lee, B. L. Choi, Y. Kuk, J. M. Kim and K. Kim, *Nature Photonics* **5** (3), 176-182 (2011).
40. A. Irwin, *Nature* **515** (553), 268-270 (2018).
41. K. M. Zielinska-Dabkowska, *Nature* **515** (553), 274-276 (2018).
42. F. Wu, C. Lin, C. Wei, C. Chen, H. Huang and C. Ho, *IEEE Photonics Technology Letters* **24** (19), 1730-1732 (2012).
43. C.-H. Yeh, Y.-L. Liu and C.-W. Chow, *Opt. Express* **21** (22), 26192-26197 (2013).
44. H. Li, X. Chen, J. Guo and H. Chen, *Opt. Express* **22** (22), 27203-27213 (2014).
45. K. Saxena, V. K. Jain and D. S. Mehta, *Optical Materials* **32** (1), 221-233 (2009).
46. W. Davis and Y. Ohno, *Toward an improved color rendering metric*. (SPIE, 2005).
47. S. Li, Z. Shi, F. Zhang, L. Wang, Z. Ma, D. Yang, Z. Yao, D. Wu, T.-T. Xu, Y. Tian, Y. Zhang, C. Shan and X. J. Li, *Chemistry of Materials* **31** (11), 3917-3928 (2019).
48. C. B. Murray, D. J. Norris and M. G. Bawendi, *Journal of the American Chemical Society* **115** (19), 8706-8715 (1993).
49. Q. Zhou, Z. Bai, L. Lu and H. Zhong, *Chinese Optics* **8** (3), 313-328 (2015).
50. A. J. Wilkins, I. Nimmo-Smith, A. I. Slater and L. Bedocs, *Lighting Research & Technology* **21** (1), 11-18 (1989).
51. Y. Shirasaki, G. J. Supran, M. G. Bawendi and V. Bulović, *Nature Photonics* **7** (1), 13-23 (2013).

52. H. Zhang, Q. Su and S. Chen, *Journal of Information Display* **20** (4), 169-180 (2019).
53. B. Hou, Y. Li, Y. Liu, B. Yuan, M. Jia and F. Jiang, *CrystEngComm* **11** (9), 1789-1792 (2009).
54. B. Hou, Y. Liu, Y. Li, B. Yuan, M. Jia and F. Jiang, *Materials Science and Engineering: B* **177** (5), 411-415 (2012).
55. L. N. Quan, B. P. Rand, R. H. Friend, S. G. Mhaisalkar, T.-W. Lee and E. H. Sargent, *Chemical Reviews* **119** (12), 7444-7477 (2019).
56. W.-S. Song, J.-H. Kim, J.-H. Lee, H.-S. Lee, Y. R. Do and H. Yang, *Journal of Materials Chemistry* **22** (41), 21901-21908 (2012).
57. C. R. Kagan, C. B. Murray and M. G. Bawendi, *Physical Review B* **54** (12), 8633-8643 (1996).
58. F. Xu, X. Ma, C. R. Haughn, J. Benavides, M. F. Doty and S. G. Cloutier, *ACS Nano* **5** (12), 9950-9957 (2011).
59. J.-M. Caruge, J. E. Halpert, V. Bulović and M. G. Bawendi, *Nano Letters* **6** (12), 2991-2994 (2006).
60. V. Wood, M. J. Panzer, J. E. Halpert, J. M. Caruge, M. G. Bawendi and V. Bulović, *ACS Nano* **3** (11), 3581-3586 (2009).
61. J. W. Stouwdam and R. A. J. Janssen, *Advanced Materials* **21** (28), 2916-2920 (2009).
62. H. Huang, A. Dorn, G. P. Nair, V. Bulović and M. G. Bawendi, *Nano Letters* **7** (12), 3781-3786 (2007).
63. S. Nakamura, T. Mukai and M. Senoh, *Applied Physics Letters* **64** (13), 1687-1689 (1994).
64. M. R. Krames, O. B. Shchekin, R. Mueller-Mach, G. O. Mueller, L. Zhou, G. Harbers and M. G. Craford, *Journal of Display Technology* **3** (2), 160-175 (2007).
65. H. V. Demir, S. Nizamoglu, T. Erdem, E. Mutlugun, N. Gaponik and A. Eychmüller, *Nano Today* **6** (6), 632-647 (2011).
66. T. Erdem and V. Demir Hilmi, in *Nanophotonics* (2016), Vol. 5, pp. 74.
67. B. Hou, D. Parker, G. P. Kissling, J. A. Jones, D. Cherns and D. J. Fermín, *The Journal of Physical Chemistry C* **117** (13), 6814-6820 (2013).
68. C. Hsueh-Shih, H. Cheng-Kuo and H. Hsin-Yen, *IEEE Photonics Technology Letters* **18** (1), 193-195 (2006).
69. H. S. Jang, H. Yang, S. W. Kim, J. Y. Han, S.-G. Lee and D. Y. Jeon, *Advanced Materials* **20** (14), 2696-2702 (2008).
70. J. Ziegler, S. Xu, E. Kucur, F. Meister, M. Batentschuk, F. Gindele and T. Nann, *Advanced Materials* **20** (21), 4068-4073 (2008).
71. B. O. Dabbousi, J. Rodriguez-Viejo, F. V. Mikulec, J. R. Heine, H. Mattoussi, R. Ober, K. F. Jensen and M. G. Bawendi, *The Journal of Physical Chemistry B* **101** (46), 9463-9475 (1997).
72. A. M. Smith, A. M. Mohs and S. Nie, *Nature Nanotechnology* **4** (1), 56-63 (2009).
73. D. V. Talapin, I. Mekis, S. Götzinger, A. Kornowski, O. Benson and H. Weller, *The Journal of Physical Chemistry B* **108** (49), 18826-18831 (2004).
74. S. Yu, X.-B. Fan, X. Wang, J. Li, Q. Zhang, A. Xia, S. Wei, L.-Z. Wu, Y. Zhou and

- G. R. Patzke, *Nature Communications* **9** (1), 4009 (2018).
75. J. Lim, M. Park, W. K. Bae, D. Lee, S. Lee, C. Lee and K. Char, *ACS Nano* **7** (10), 9019-9026 (2013).
76. J. Zhang, J. Wang, T. Yan, Y. Peng, D. Xu and D. Deng, *Journal of Materials Chemistry B* **5** (41), 8152-8160 (2017).
77. P. Ramasamy, K.-J. Ko, J.-W. Kang and J.-S. Lee, *Chemistry of Materials* **30** (11), 3643-3647 (2018).
78. D.-E. Nam, W.-S. Song and H. Yang, *Journal of Materials Chemistry* **21** (45), 18220-18226 (2011).
79. Y.-K. Kim, S.-H. Ahn, K. Chung, Y.-S. Cho and C.-J. Choi, *Journal of Materials Chemistry* **22** (4), 1516-1520 (2012).
80. W.-S. Song and H. Yang, *Applied Physics Letters* **100** (18), 183104 (2012).
81. H. Zhong, Z. Bai and B. Zou, *The Journal of Physical Chemistry Letters* **3** (21), 3167-3175 (2012).
82. B. Chen, N. Pradhan and H. Zhong, *The Journal of Physical Chemistry Letters* **9** (2), 435-445 (2018).
83. B. Chen, H. Zhong, M. Wang, R. Liu and B. Zou, *Nanoscale* **5** (8), 3514-3519 (2013).
84. D. W. de Quilettes, S. M. Vorpahl, S. D. Stranks, H. Nagaoka, G. E. Eperon, M. E. Ziffer, H. J. Snaith and D. S. Ginger, *Science* **348** (6235), 683 (2015).
85. N. J. Jeon, J. H. Noh, W. S. Yang, Y. C. Kim, S. Ryu, J. Seo and S. I. Seok, *Nature* **517** (7535), 476-480 (2015).
86. W. S. Yang, B.-W. Park, E. H. Jung, N. J. Jeon, Y. C. Kim, D. U. Lee, S. S. Shin, J. Seo, E. K. Kim, J. H. Noh and S. I. Seok, *Science* **356** (6345), 1376 (2017).
87. N. J. Jeon, H. Na, E. H. Jung, T.-Y. Yang, Y. G. Lee, G. Kim, H.-W. Shin, S. I. Seok, J. Lee and J. Seo, *Nature Energy* **3** (8), 682-689 (2018).
88. J. Luo, X. Wang, S. Li, J. Liu, Y. Guo, G. Niu, L. Yao, Y. Fu, L. Gao, Q. Dong, C. Zhao, M. Leng, F. Ma, W. Liang, L. Wang, S. Jin, J. Han, L. Zhang, J. Etheridge, J. Wang, Y. Yan, E. H. Sargent and J. Tang, *Nature* **563** (7732), 541-545 (2018).
89. S. Coe, W.-K. Woo, M. Bawendi and V. Bulović, *Nature* **420** (6917), 800-803 (2002).
90. H. Yang and P. H. Holloway, *The Journal of Physical Chemistry B* **107** (36), 9705-9710 (2003).
91. B. Hou, D. Benito-Alifonso, R. Webster, D. Cherns, M. C. Galan and D. J. Fermín, *Journal of Materials Chemistry A* **2** (19), 6879-6886 (2014).
92. D. Benito-Alifonso, S. Tremel, B. Hou, H. Lockyear, J. Mantell, D. J. Fermin, P. Verkade, M. Berry and M. C. Galan, *Angewandte Chemie International Edition* **53** (3), 810-814 (2014).
93. Y. Li, A. Rizzo, M. Mazzeo, L. Carbone, L. Manna, R. Cingolani and G. Gigli, *Journal of Applied Physics* **97** (11) (2005).
94. Y. Q. Li, A. Rizzo, R. Cingolani and G. Gigli, *Advanced Materials* **18** (19), 2545-2548 (2006).
95. W. K. Bae, J. Kwak, J. Lim, D. Lee, M. K. Nam, K. Char, C. Lee and S. Lee, *Nano Letters* **10** (7), 2368-2373 (2010).

96. M. K. Choi, J. Yang, K. Kang, D. C. Kim, C. Choi, C. Park, S. J. Kim, S. I. Chae, T.-H. Kim, J. H. Kim, T. Hyeon and D.-H. Kim, *Nature Communications* **6** (1), 7149 (2015).
97. K.-H. Lee, C.-Y. Han, E.-P. Jang, J.-H. Jo, S. Hong, J. Y. Hwang, E. Choi, J.-H. Hwang and H. Yang, *Nanoscale* **10** (14), 6300-6305 (2018).
98. H. Zhang, S. Wang, X. Sun and S. Chen, *Journal of the Society for Information Display* **25** (3), 143-150 (2017).
99. W. K. Bae, J. Lim, D. Lee, M. Park, H. Lee, J. Kwak, K. Char, C. Lee and S. Lee, *Advanced Materials* **26** (37), 6387-6393 (2014).
100. L. Wang, J. Lin, Y. Hu, X. Guo, Y. Lv, Z. Tang, J. Zhao, Y. Fan, N. Zhang, Y. Wang and X. Liu, *ACS Applied Materials & Interfaces* **9** (44), 38755-38760 (2017).
101. H. Zhang, X. Sun and S. Chen, *Advanced Functional Materials* **27** (21), 1700610 (2017).
102. H. Zhang, S. Chen and X. W. Sun, *ACS Nano* **12** (1), 697-704 (2018).
103. L. S. Liao, W. K. Slusarek, T. K. Hatwar, M. L. Ricks and D. L. Comfort, *Advanced Materials* **20** (2), 324-329 (2008).
104. S. Lee, H. Shin and J.-J. Kim, *Advanced Materials* **26** (33), 5864-5868 (2014).
105. T. Chiba, Y.-J. Pu and J. Kido, *Advanced Materials* **27** (32), 4681-4687 (2015).
106. C. Jiang, J. Zou, Y. Liu, C. Song, Z. He, Z. Zhong, J. Wang, H.-L. Yip, J. Peng and Y. Cao, *ACS Nano* **12** (6), 6040-6049 (2018).
107. S. Hamwi, J. Meyer, M. Kröger, T. Winkler, M. Witte, T. Riedl, A. Kahn and W. Kowalsky, *Advanced Functional Materials* **20** (11), 1762-1766 (2010).
108. J. Meyer, S. Hamwi, M. Kröger, W. Kowalsky, T. Riedl and A. Kahn, *Advanced Materials* **24** (40), 5408-5427 (2012).
109. B. Blackman, D. M. Battaglia, T. D. Mishima, M. B. Johnson and X. Peng, *Chemistry of Materials* **19** (15), 3815-3821 (2007).
110. A. K. Gooding, D. E. Gómez and P. Mulvaney, *ACS Nano* **2** (4), 669-676 (2008).
111. W. K. Bae, K. Char, H. Hur and S. Lee, *Chemistry of Materials* **20** (2), 531-539 (2008).
112. D. V. Talapin, J.-S. Lee, M. V. Kovalenko and E. V. Shevchenko, *Chemical Reviews* **110** (1), 389-458 (2010).
113. L. Li and P. Reiss, *Journal of the American Chemical Society* **130** (35), 11588-11589 (2008).
114. R. Xie and X. Peng, *Journal of the American Chemical Society* **131** (30), 10645-10651 (2009).
115. P. M. Allen, B. J. Walker and M. G. Bawendi, *Angewandte Chemie International Edition* **49** (4), 760-762 (2010).
116. X. Yang, Y. Divayana, D. Zhao, K. Swee Leck, F. Lu, S. Tiam Tan, A. Putu Abiyasa, Y. Zhao, H. Volkan Demir and X. Wei Sun, *Applied Physics Letters* **101** (23), 233110 (2012).
117. H. Y. Kim, Y. J. Park, J. Kim, C. J. Han, J. Lee, Y. Kim, T. Greco, C. Ippen, A. Wedel, B.-K. Ju and M. S. Oh, *Advanced Functional Materials* **26** (20), 3454-3461 (2016).
118. H. C. Wang, H. Zhang, H. Y. Chen, H. C. Yeh, M. R. Tseng, R. J. Chung, S. Chen

- and R. S. Liu, *Small* **13** (13), 1603962 (2017).
119. F. Cao, S. Wang, F. Wang, Q. Wu, D. Zhao and X. Yang, *Chemistry of Materials* **30** (21), 8002-8007 (2018).
120. H. Zhang, X. Ma, Q. Lin, Z. Zeng, H. Wang, L. S. Li, H. Shen, Y. Jia and Z. Du, *The Journal of Physical Chemistry Letters* **11** (3), 960-967 (2020).
121. H. Zhong, Z. Wang, E. Bovero, Z. Lu, F. C. J. M. van Veggel and G. D. Scholes, *The Journal of Physical Chemistry C* **115** (25), 12396-12402 (2011).
122. Z. Tan, Y. Zhang, C. Xie, H. Su, J. Liu, C. Zhang, N. Dellas, S. E. Mohney, Y. Wang, J. Wang and J. Xu, *Advanced Materials* **23** (31), 3553-3558 (2011).
123. B. Chen, H. Zhong, W. Zhang, Z. a. Tan, Y. Li, C. Yu, T. Zhai, Y. Bando, S. Yang and B. Zou, *Advanced Functional Materials* **22** (10), 2081-2088 (2012).
124. W. Zhang, Q. Lou, W. Ji, J. Zhao and X. Zhong, *Chemistry of Materials* **26** (2), 1204-1212 (2014).
125. S. Cao, W. Ji, J. Zhao, W. Yang, C. Li and J. Zheng, *Journal of Materials Chemistry C* **4** (3), 581-588 (2016).
126. Y. Zhang, C. Xie, H. Su, J. Liu, S. Pickering, Y. Wang, W. W. Yu, J. Wang, Y. Wang, J.-i. Hahn, N. Dellas, S. E. Mohney and J. Xu, *Nano Letters* **11** (2), 329-332 (2011).
127. Z. Liu, A. Tang, Y. Xie, Z. Guan, Y. Chen and F. Teng, *Organic Electronics* **45**, 20-25 (2017).
128. Z. Zhang, D. Liu, D. Li, K. Huang, Y. Zhang, Z. Shi, R. Xie, M.-Y. Han, Y. Wang and W. Yang, *Chemistry of Materials* **27** (4), 1405-1411 (2015).
129. M. J. Bowers, J. R. McBride and S. J. Rosenthal, *Journal of the American Chemical Society* **127** (44), 15378-15379 (2005).
130. M. A. Schreuder, K. Xiao, I. N. Ivanov, S. M. Weiss and S. J. Rosenthal, *Nano Letters* **10** (2), 573-576 (2010).
131. M. Bidikoudi, E. Fresta and R. D. Costa, *Chem Commun (Camb)* **54** (59), 8150-8169 (2018).
132. H. C. Wang, Z. Bao, H. Y. Tsai, A. C. Tang and R. S. Liu, *Small* **14** (1) (2018).
133. O. Ergen, S. M. Gilbert, T. Pham, Sally J. Turner, Mark Tian Z. Tan, Marcus A. Worsley and A. Zettl, *Nature Materials* **16** (5), 522-525 (2017).
134. X. Zheng, Y. Hou, C. Bao, J. Yin, F. Yuan, Z. Huang, K. Song, J. Liu, J. Troughton, N. Gasparini, C. Zhou, Y. Lin, D.-J. Xue, B. Chen, A. K. Johnston, N. Wei, M. N. Hedhili, M. Wei, A. Y. Alsalloum, P. Maity, B. Turedi, C. Yang, D. Baran, T. D. Anthopoulos, Y. Han, Z.-H. Lu, O. F. Mohammed, F. Gao, E. H. Sargent and O. M. Bakr, *Nature Energy* **5** (2), 131-140 (2020).
135. N. Wang, L. Cheng, R. Ge, S. Zhang, Y. Miao, W. Zou, C. Yi, Y. Sun, Y. Cao, R. Yang, Y. Wei, Q. Guo, Y. Ke, M. Yu, Y. Jin, Y. Liu, Q. Ding, D. Di, L. Yang, G. Xing, H. Tian, C. Jin, F. Gao, R. H. Friend, J. Wang and W. Huang, *Nature Photonics* **10** (11), 699-704 (2016).
136. K. Lin, J. Xing, L. N. Quan, F. P. G. de Arquer, X. Gong, J. Lu, L. Xie, W. Zhao, D. Zhang, C. Yan, W. Li, X. Liu, Y. Lu, J. Kirman, E. H. Sargent, Q. Xiong and Z. Wei, *Nature* **562** (7726), 245-248 (2018).
137. C. Li, H. Wang, F. Wang, T. Li, M. Xu, H. Wang, Z. Wang, X. Zhan, W. Hu

- and L. Shen, *Light: Science & Applications* **9** (1), 31 (2020).
138. L. Gao, L. N. Quan, F. P. García de Arquer, Y. Zhao, R. Munir, A. Proppe, R. Quintero-Bermudez, C. Zou, Z. Yang, M. I. Saidaminov, O. Voznyy, S. Kinger, Z. Lu, S. O. Kelley, A. Amassian, J. Tang and E. H. Sargent, *Nature Photonics* **14** (4), 227-233 (2020).
  139. Z.-K. Tan, R. S. Moghaddam, M. L. Lai, P. Docampo, R. Higler, F. Deschler, M. Price, A. Sadhanala, L. M. Pazos, D. Credgington, F. Hanusch, T. Bein, H. J. Snaith and R. H. Friend, *Nature Nanotechnology* **9** (9), 687-692 (2014).
  140. J. Wang, N. Wang, Y. Jin, J. Si, Z.-K. Tan, H. Du, L. Cheng, X. Dai, S. Bai, H. He, Z. Ye, M. L. Lai, R. H. Friend and W. Huang, *Advanced Materials* **27** (14), 2311-2316 (2015).
  141. J. Song, J. Li, X. Li, L. Xu, Y. Dong and H. Zeng, *Advanced Materials* **27** (44), 7162-7167 (2015).
  142. E.-P. Yao, Z. Yang, L. Meng, P. Sun, S. Dong, Y. Yang and Y. Yang, *Advanced Materials* **29** (23), 1606859 (2017).
  143. J. Mao, H. Lin, F. Ye, M. Qin, J. M. Burkhartsmeier, H. Zhang, X. Lu, K. S. Wong and W. C. H. Choy, *ACS Nano* **12** (10), 10486-10492 (2018).
  144. H. Cho, Y.-H. Kim, C. Wolf, H.-D. Lee and T.-W. Lee, *Advanced Materials* **30** (42), 1704587 (2018).
  145. J. F. Galisteo-López, M. Anaya, M. E. Calvo and H. Míguez, *The Journal of Physical Chemistry Letters* **6** (12), 2200-2205 (2015).
  146. N. Ahn, K. Kwak, M. S. Jang, H. Yoon, B. Y. Lee, J.-K. Lee, P. V. Pikhitsa, J. Byun and M. Choi, *Nature Communications* **7** (1), 13422 (2016).
  147. D. Bryant, N. Aristidou, S. Pont, I. Sanchez-Molina, T. Chotchunangatchaval, S. Wheeler, J. R. Durrant and S. A. Haque, *Energy & Environmental Science* **9** (5), 1655-1660 (2016).
  148. S. Xu, J. Ziegler and T. Nann, *Journal of Materials Chemistry* **18** (23), 2653-2656 (2008).
  149. E. Jang, S. Jun, H. Jang, J. Lim, B. Kim and Y. Kim, *Advanced Materials* **22** (28), 3076-3080 (2010).
  150. P. T. K. Chin, C. de Mello Donegá, S. S. van Bavel, S. C. J. Meskers, N. A. J. M. Sommerdijk and R. A. J. Janssen, *Journal of the American Chemical Society* **129** (48), 14880-14886 (2007).
  151. P. Jing, J. Zheng, M. Ikezawa, X. Liu, S. Lv, X. Kong, J. Zhao and Y. Masumoto, *The Journal of Physical Chemistry C* **113** (31), 13545-13550 (2009).
  152. R. Xie, U. Kolb, J. Li, T. Basché and A. Mews, *Journal of the American Chemical Society* **127** (20), 7480-7488 (2005).
  153. F. Di Stasio, S. Christodoulou, N. Huo and G. Konstantatos, *Chemistry of Materials* **29** (18), 7663-7667 (2017).
  154. J. Pan, Y. Shang, J. Yin, M. De Bastiani, W. Peng, I. Dursun, L. Sinatra, A. M. El-Zohry, M. N. Hedhili, A.-H. Emwas, O. F. Mohammed, Z. Ning and O. M. Bakr, *Journal of the American Chemical Society* **140** (2), 562-565 (2018).
  155. S. Kumar, J. Jagielski, T. Tian, N. Kallikounis, W.-C. Lee and C.-J. Shih, *ACS Energy Letters* **4** (1), 118-125 (2019).

156. C.-Y. Han, S.-H. Lee, S.-W. Song, S.-Y. Yoon, J.-H. Jo, D.-Y. Jo, H.-M. Kim, B.-J. Lee, H.-S. Kim and H. Yang, *ACS Energy Letters*, 1568-1576 (2020).
157. K.-H. Kim, J.-H. Jo, D.-Y. Jo, C.-Y. Han, S.-Y. Yoon, Y. Kim, Y.-H. Kim, Y. H. Ko, S. W. Kim, C. Lee and H. Yang, *Chemistry of Materials* **32** (8), 3537-3544 (2020).
158. F. Yuan, Y.-K. Wang, G. Sharma, Y. Dong, X. Zheng, P. Li, A. Johnston, G. Bappi, J. Z. Fan, H. Kung, B. Chen, M. I. Saidaminov, K. Singh, O. Voznyy, O. M. Bakr, Z.-H. Lu and E. H. Sargent, *Nature Photonics* **14** (3), 171-176 (2020).
159. D.-Y. Jo and H. Yang, *Chemical Communications* **52** (4), 709-712 (2016).
160. P. He, Y. Shi, T. Meng, T. Yuan, Y. Li, X. Li, Y. Zhang, L. Fan and S. Yang, *Nanoscale* **12** (8), 4826-4832 (2020).
161. F. Yuan, Z. Wang, X. Li, Y. Li, Z. a. Tan, L. Fan and S. Yang, *Advanced Materials* **29** (3), 1604436 (2017).
162. H. Jia, Z. Wang, T. Yuan, F. Yuan, X. Li, Y. Li, Z. a. Tan, L. Fan and S. Yang, *Advanced Science* **6** (13), 1900397 (2019).
163. Z. Luo, G. Qi, K. Chen, M. Zou, L. Yuwen, X. Zhang, W. Huang and L. Wang, *Advanced Functional Materials* **26** (16), 2739-2744 (2016).
164. D. I. Son, B. W. Kwon, D. H. Park, W.-S. Seo, Y. Yi, B. Angadi, C.-L. Lee and W. K. Choi, *Nature Nanotechnology* **7** (7), 465-471 (2012).
165. Y.-X. Chen, D. Lu, G.-G. Wang, J. Huangfu, Q.-B. Wu, X.-F. Wang, L.-F. Liu, D.-M. Ye, B. Yan and J. Han, *ACS Sustainable Chemistry & Engineering* (2020).
166. J. Pu and T. Takenobu, *Advanced Materials* **30** (33), 1707627 (2018).
167. D.-H. Lien, M. Amani, S. B. Desai, G. H. Ahn, K. Han, J.-H. He, J. W. Ager, M. C. Wu and A. Javey, *Nature Communications* **9** (1), 1229 (2018).
168. C. Palacios-Berraquero, M. Barbone, D. M. Kara, X. Chen, I. Goykhman, D. Yoon, A. K. Ott, J. Beitner, K. Watanabe, T. Taniguchi, A. C. Ferrari and M. Atatüre, *Nature Communications* **7** (1), 12978 (2016).
169. F. Withers, O. Del Pozo-Zamudio, A. Mishchenko, A. P. Rooney, A. Gholinia, K. Watanabe, T. Taniguchi, S. J. Haigh, A. K. Geim, A. I. Tartakovskii and K. S. Novoselov, *Nature Materials* **14** (3), 301-306 (2015).

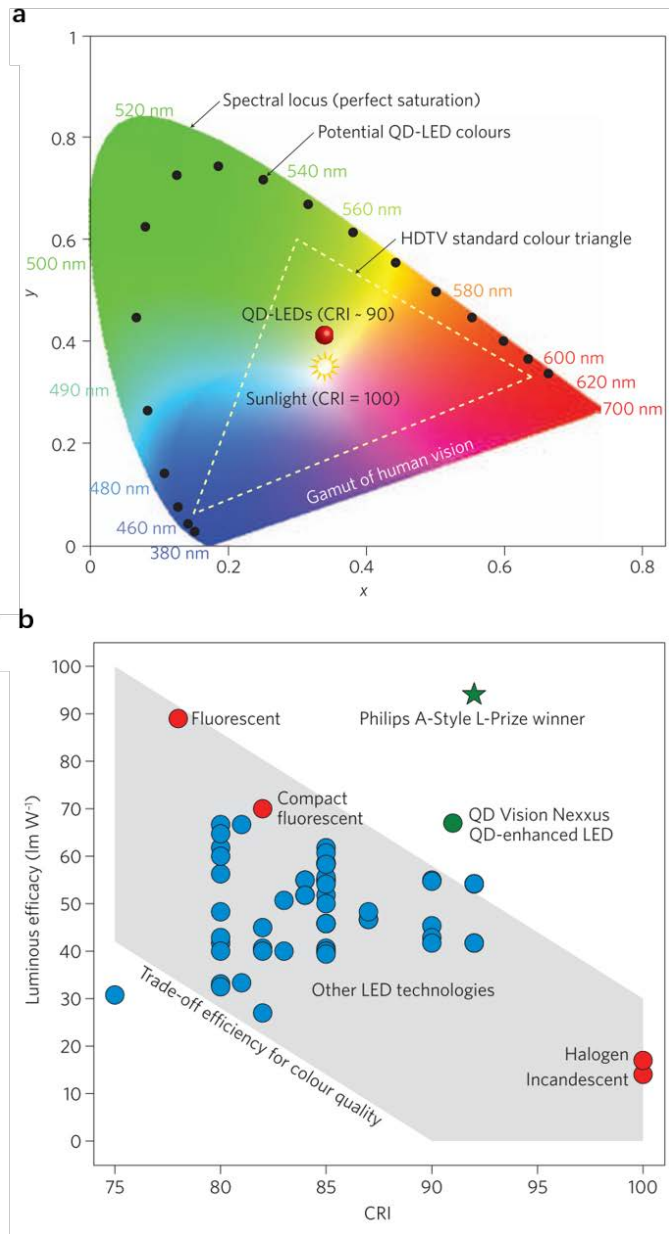


**Figure 1.** (a) CIE chromaticity diagram showing the spectral purity of QDs enabling a colour gamut (dotted line) more substantial than the high-definition television (HDTV) standard (dashed line). (b) Plot showing the luminous efficacy and CRI of various commercially available lighting solutions. Copyright 2013. Springer Nature.

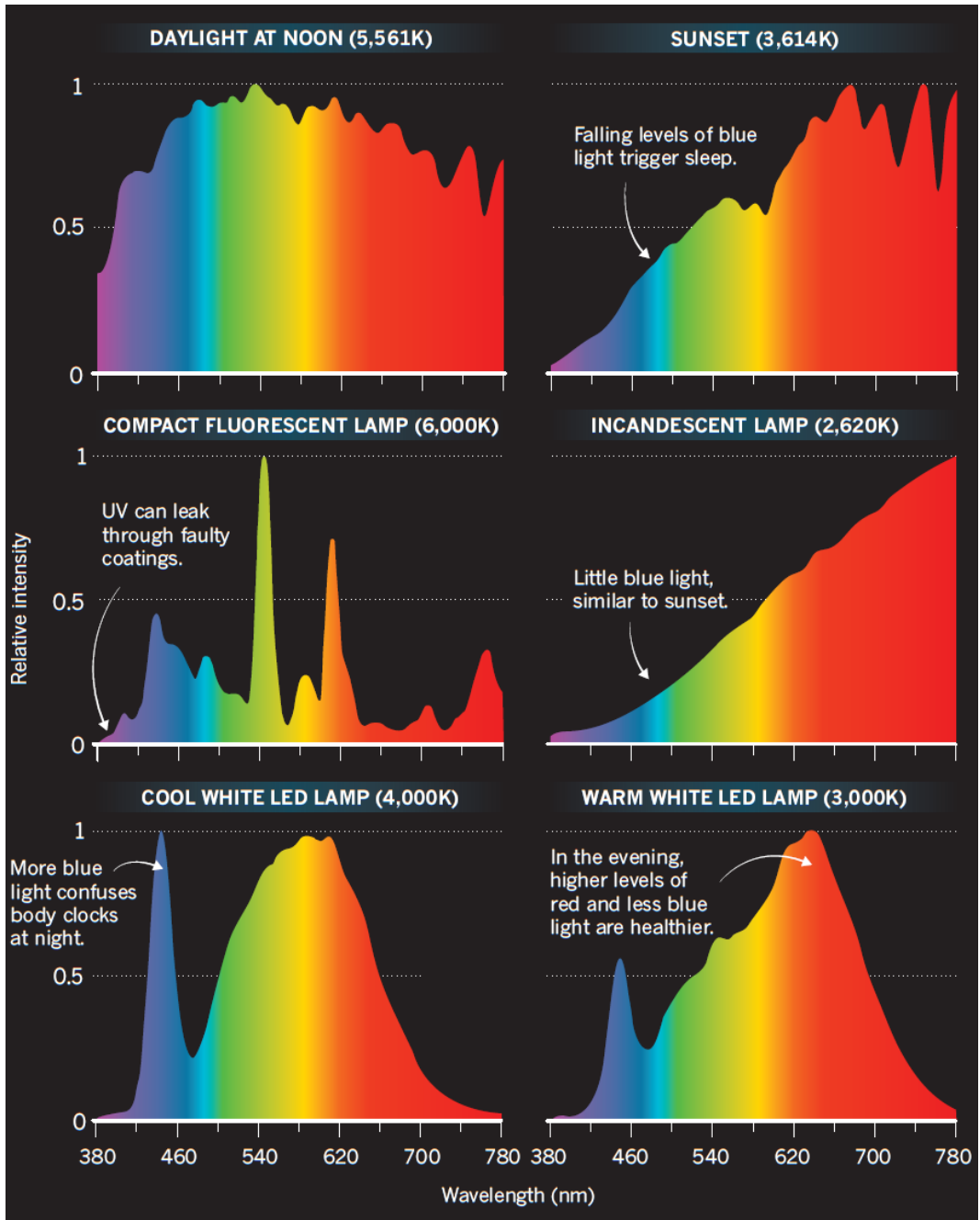


**Figure 2.** Different spectral distribution from various white lighting source. Copyright 2018. Springer Nature.

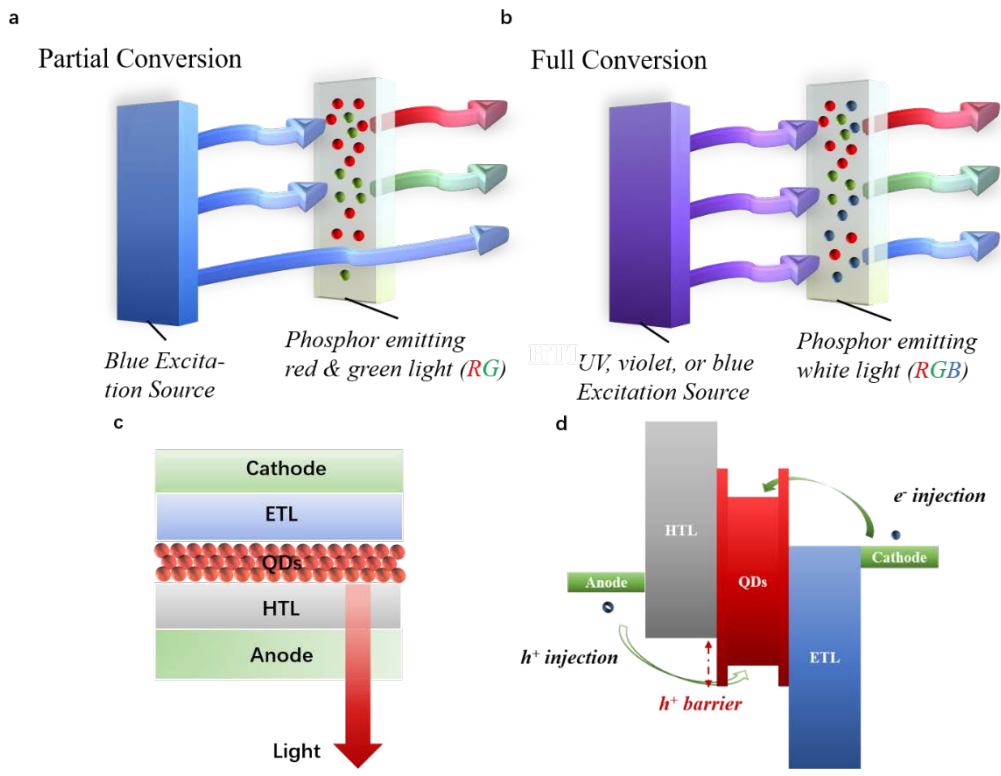


**Figure 3.** (a) Partial light conversion in pc-WQLEDs. (b) Full light conversion in pc-WQLEDs. (c) Configuration of single mixed-QD WQLEDs, with schematic energy level showing injection of hole and electron.

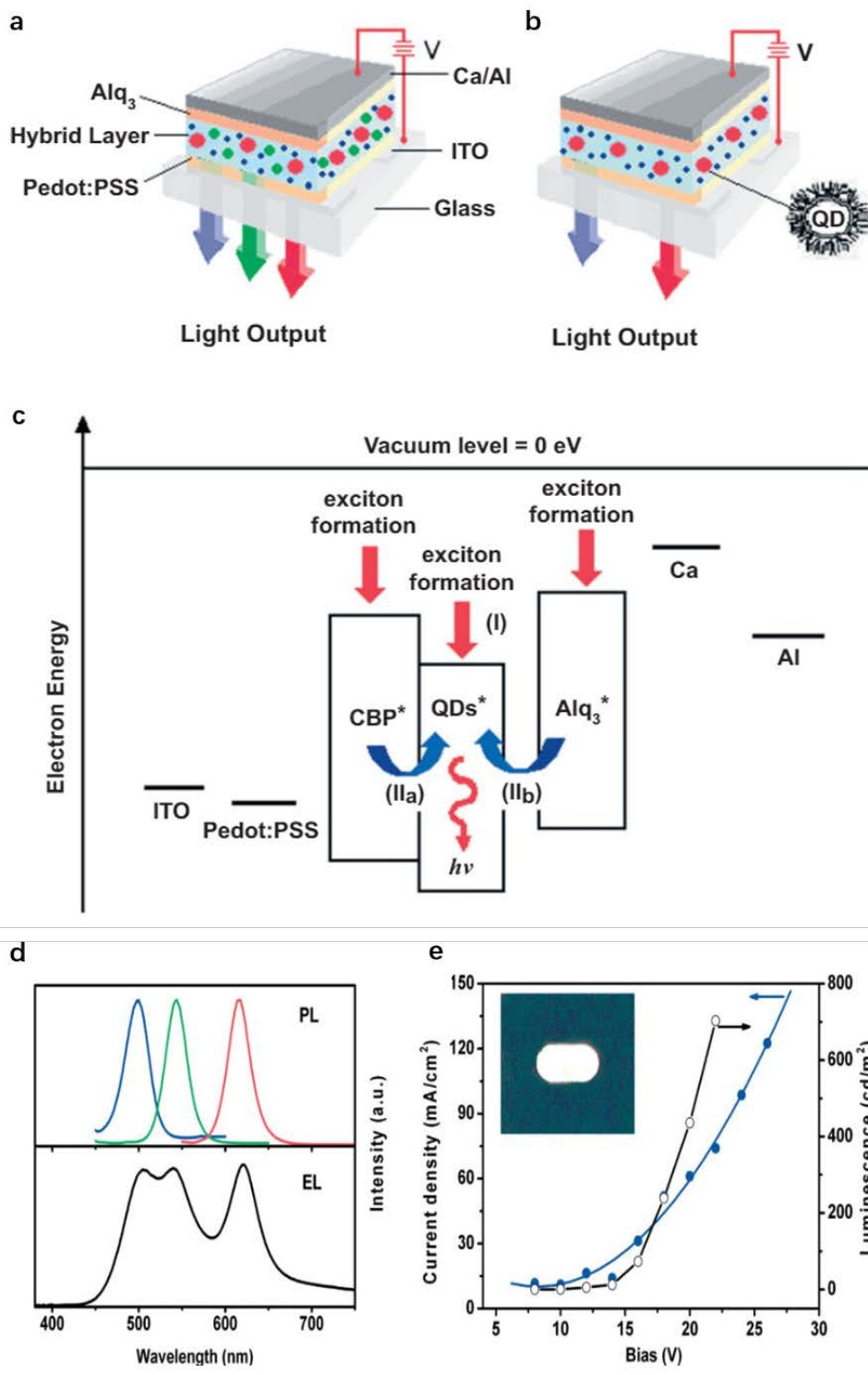


**Figure 4.** (a) The structure of the device ITO//PEDOT:PSS//CBP:QDs(B/G R)//Alq<sub>3</sub>//Ca/Al. (b)The structure ITO//PEDOT:PSS//CBP:QDs(B/R)//Alq<sub>3</sub>//Ca/Al. (c) Energy level diagram of devices and possible exciton creation mechanisms on the QDs: I) charge trapping and II) Förster energy transfer. (d) EL and PL spectra and characteristics of the ternary mixed-QD WQLEDs. (e) Current-voltage and current-luminescence curves of WQLEDs, with an image of the working device as inset. Copyright 2006, Wiley-VCH.

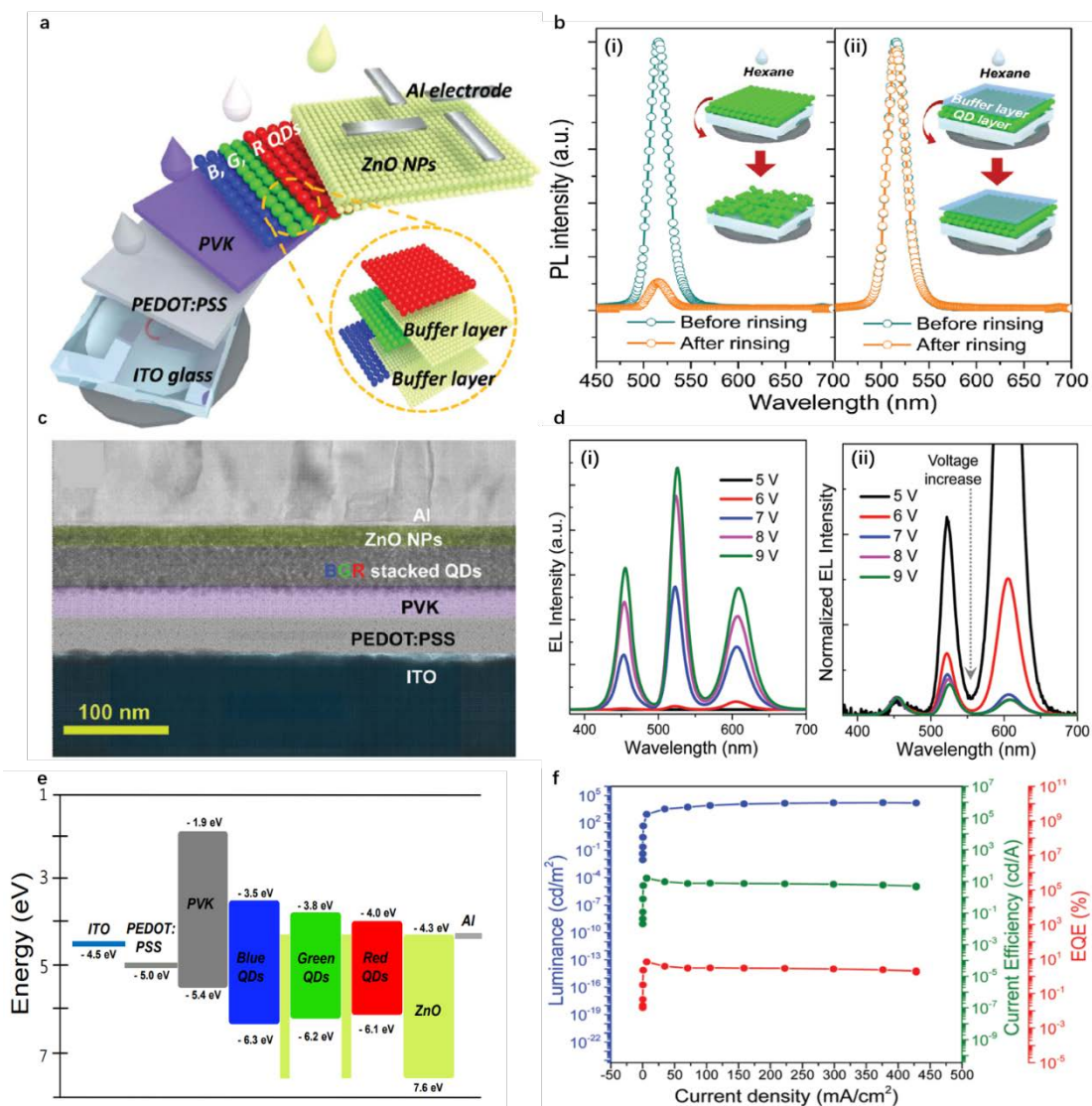


**Figure 5.** (a) Structure of multi-layered WQLEDs. (b) Comparison of PL spectra of green QD films (i) with and (ii) without ZnO inserted layer before and after hexane rinsing. (c) Cross-sectional TEM image of multi-layered WQLEDs. (d) Voltage-dependence of EL evolution in a device, (i) as-obtained (ii) Normalised. (e) Diagram of energy level in WQLEDs. (f) Variations in luminance, CE and EQE with the current density of multi-layered WQLEDs. Copyright 2018, The Royal Society of Chemistry.

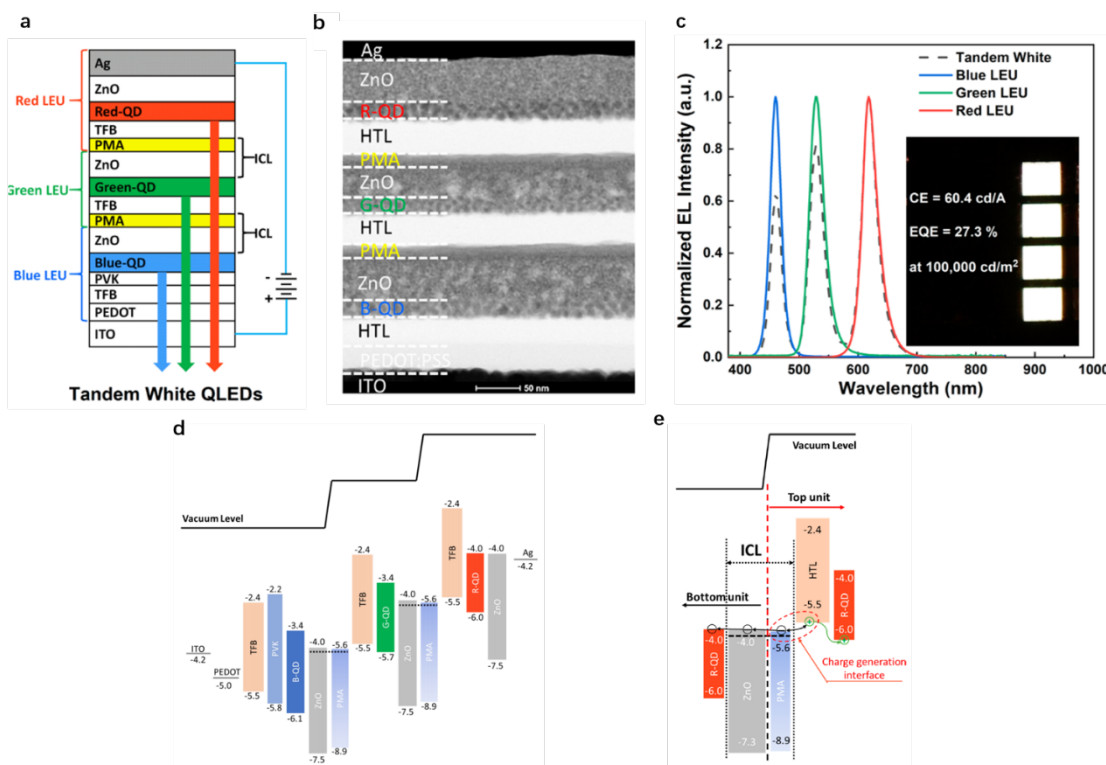


**Figure 6.** (a) Architecture of tandem WQLEDs. (b) Cross-sectional STEM of tandem WQLEDs. (c) Normalised EL spectra of the device, with inset showing performance data and working images. (e) Energy level diagram of tandem WQLEDs. (e) schematic diagram of the charge generation and injection mechanism. Copyright 2018, American Chemical Society.

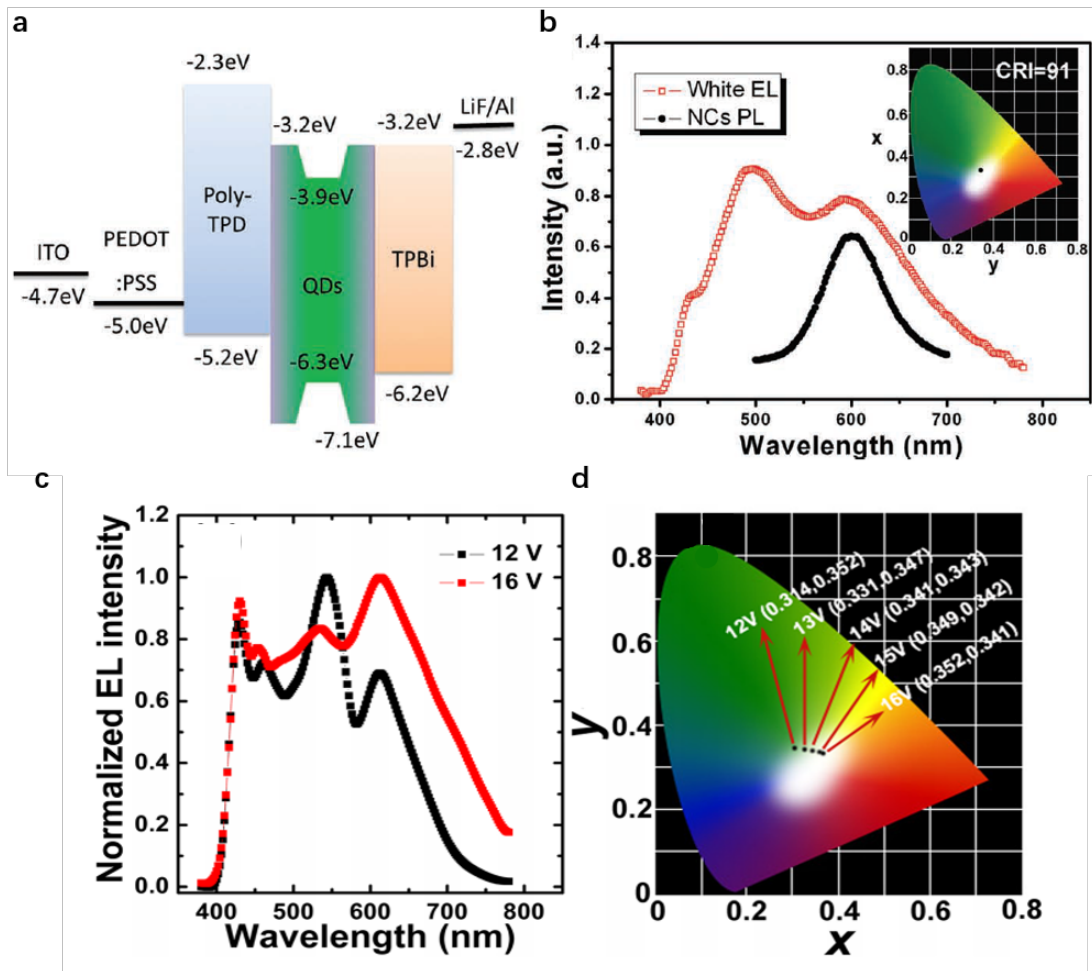


**Figure 7.** (a) Energy band diagram of InP/ZnS-based WQLEDs. (b) PL spectra of red-emitting InP/ZnS QDs and WQLEDs. (c) Normalized EL spectra of WQLEDs at 12V and 16V biases. (d) Shifts of CIE coordinates corresponding to bias variation. Copyright 2012, Wiley-VCH. Copyright 2012, American Institute of Physics.

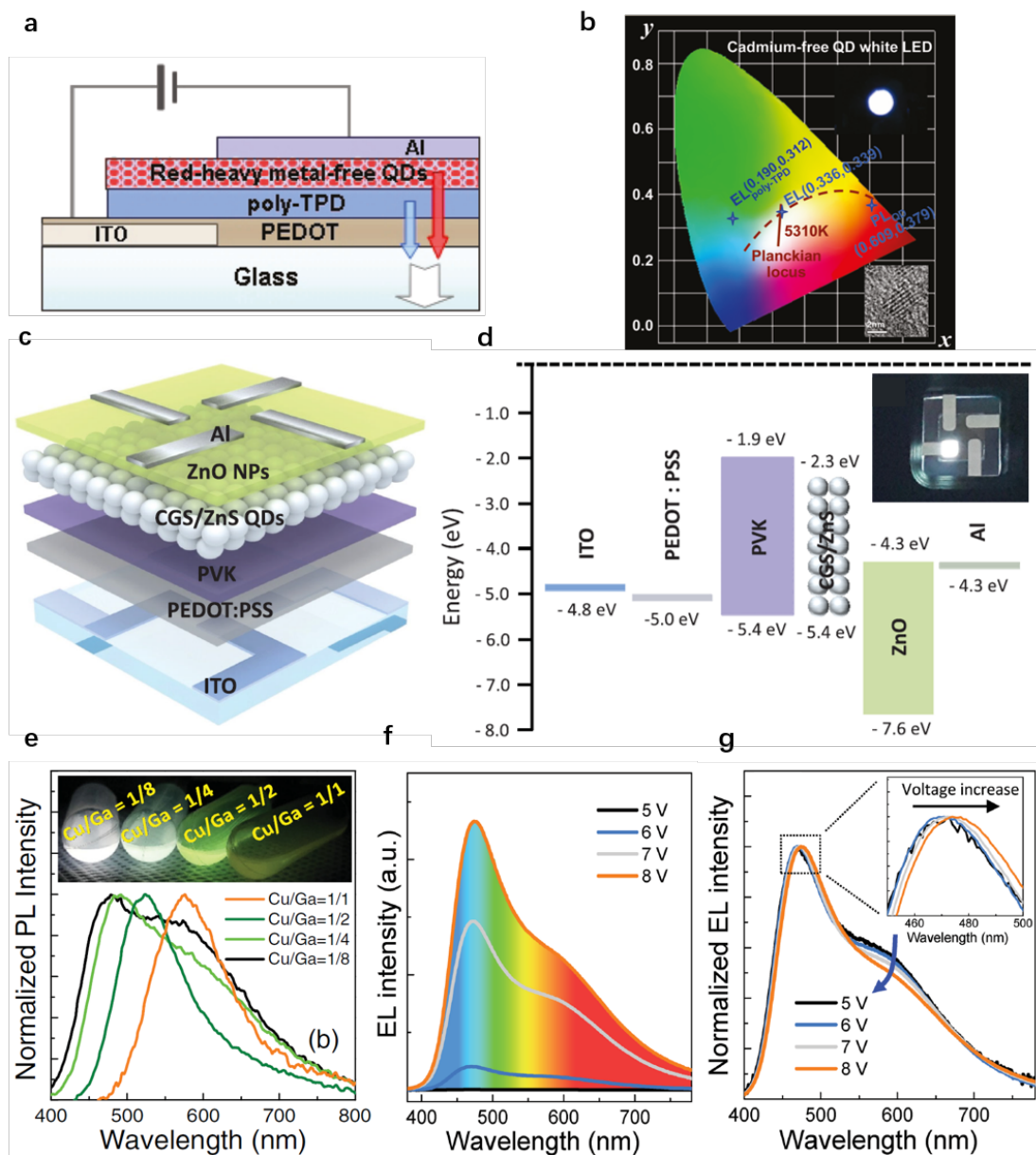


**Figure 8.** (a) Structure of the ZnCuInS/ZnS QDs/poly-TPD bilayer WQLED. (b) CIE coordinate diagram of WQLED. Insets present WQLED with the brightness of 300 cd m<sup>-2</sup> and high-resolution TEM image of ZnCuInS/ZnS QDs. (c) Device schematic. (d) Energy band diagram of single-emitter WQLEDs. Inset: an image of a device operated at 6V. (e) Normalized PL spectra of a series of CGS/ZnS QDs synthesized with different Cu/Ga ratios, with fluorescent images as inset. (f) As-collected EL spectra of devices working at different voltages. (g) Normalized EL spectra related to EL wavelengths and bias. Copyright 2011, American Chemical Society. Copyright 2016, Wiley-VCH.

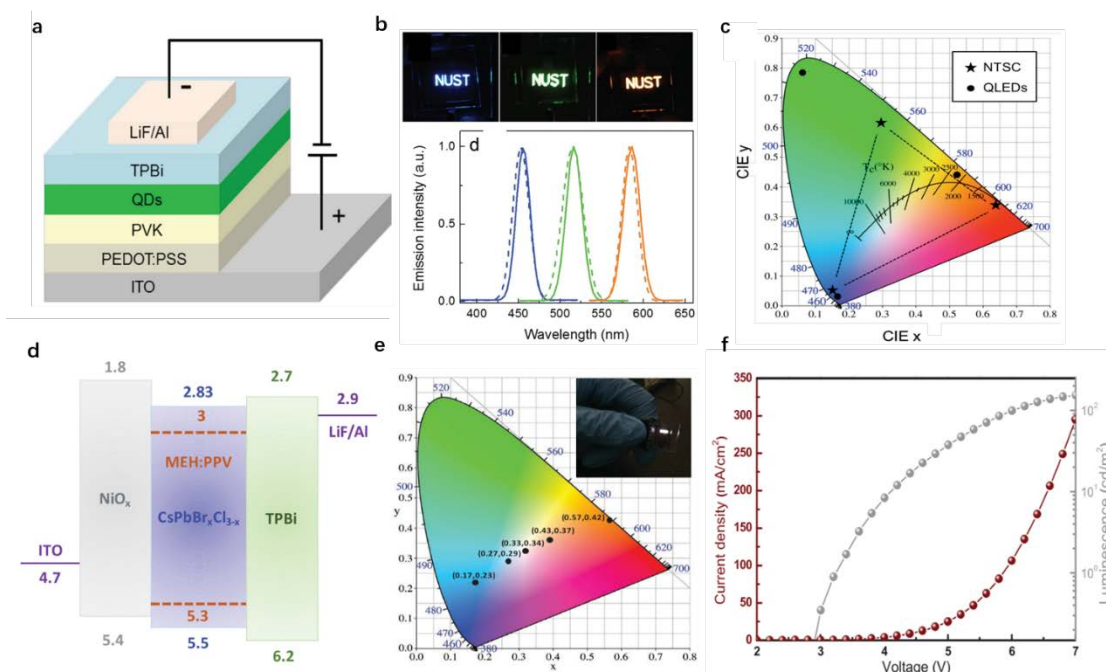


**Figure 9.** (a) Device structure of multilayer perovskite QLEDs. (b) The EL spectra (straight line) of the sample shown in inserted pictures under an applied voltage of 5.5 V, and the PL spectra (dashed line) of QDs in hexane (c) CIE coordinates of the three-colour QLEDs (circular) compared to the NTSC colour standards (stars). (d) Band structure of CsPbBr<sub>x</sub>Cl<sub>3-x</sub> nanocrystal-based blue LED. (e) CIE coordinates. (f)  $JL$ - $V$  curve, of CsPbBr<sub>x</sub>Cl<sub>3-x</sub> nanocrystal and MEH:PPV blend white LED. Copyright 2015, Wiley-VCH and Copyright 2017, Wiley-VCH.